Politecnico di Torino

Corso di Laurea
A.a. 2023/2024
Sessione di Laurea Marzo 2024

Simulation of a biomass treatment process for the production of biofuels with pressurized torrefaction and plasma gasification on Aspen Plus

Relatori:
Prof. Andrea Lanzini
PhD Omar D. Dacres

Candidati:
Tommaso Carlassara

Politecnico di Torino

Corso di Laurea
A.a. 2023/2024
Sessione di Laurea Marzo 2024

Simulation of a biomass treatment process for the production of biofuels with pressurized torrefaction and plasma gasification on Aspen Plus

Relatori:
Prof. Andrea Lanzini
PhD Omar D. Dacres

Candidati:
Tommaso Carlassara

Ai miei genitori,
per il loro costante sostegno e amore,
per i loro sforzi e sacrifici. Ma soprattutto,
per il miglior regalo che un figlio possa ricevere:
il futuro.

Abstract

Biomass is one of the most widely utilized renewable energy sources and is therefore an essential element of sustainable energy production. Different technologies for the direct and indirect utilization of biomass exist. However, biomass is still not fully exploited at its maximum potential, thus further research and development of biomass conversion are necessary.

This work aims to offer its contribution to the development of two technologies of focus: torrefaction and gasification. Specifically, the study strives to investigate alternatives to conventional biomass thermo-chemical conversion technologies, namely atmospheric torrefaction and autothermal gasification. A base case thermochemical biomass-to-liquid process, composing of 6 hierarchies is modelled in Aspen Plus for the following sub-systems: torrefaction process, gasification process, quenching, water-gas-shift, acid gas removal, Fischer-Tropsch synthesis and upgrading. The base case model is then subsequently modified with gas-pressurized torrefaction using experimental data to represent the respective process. Another variation is made to the model through converting the conventional gasification process to one that is plasma-fired.

The results and effect of the two adjustments are then discussed and compared, taking into consideration the energy yields, carbon conversion and efficiencies. A techno-economic analysis of the gas-pressurized process is also performed.

Sommario

Le biomasse sono una delle fonti di energia rinnovabile più ampiamente utilizzate e sono quindi elemento essenziale per una produzione sostenibile di energia. Diverse tecnologie esistono per lo sfruttamento diretto o indiretto delle biomasse. Ciò nonostante, le biomasse non sono ancora sfruttate al loro massimo potenziale e perciò sono necessarie ulteriori studi.

Questo lavoro ha come obbiettivo di offrire il suo contributo per lo sviluppo di due tecnologie di interesse per il trattamento delle biomasse: la torrefazione e gassificazione. Nello specifico, lo studio vuole investigare valide alternative alle convenzionali tecnologie di conversione termo-chimica delle biomasse, precisamente la torrefazione atmosferica alla gassificazione autotermica. Un modello base di un processo da biomassa a liquido è sviluppato in Aspen Plus, composto di 6 blocchi gerarchici per i seguenti sottosistemi: processo di torrefazione, gassificazione, quenching, water-gas-shift, rimozione di gas acidi, sintesi di Fischer-Tropsch e upgrade. Il modello base è successivamente modificato inserendo i dati sperimentali relativi alla torrefazione pressurizzata a gas per rappresentare il rispettivo processo, e un'ulteriore modifica è fatta convertendo il tradizionale processo di gassificazione con gassificazione al plasma.

I risultati ed effetti delle variazioni apportate sono discusse e paragonate, considerando le rese energetiche, in massa e le efficienze delle varie sezioni del processo. Viene inoltre sviluppata un'analisi tecno-ecoomica della torrefazione.

Contents

Abbreviations

TUM Technical University of Munich

HHV Higher Heating Value

LHV Lower Heating Value

PSD Particle Size Distribution

DAF Dry Ash Free

CGE Cold Gas Efficiency

WGS Water-Gas shift

AGR Acid Gas Removal

GP gas-pressurized

AP atmospheric pressure

FTS Fischer Tropsch Synthesis

BtL biomass-to-liquid

KPI key performance indicators

List of Figures

List of Tables

1. Introduction

1.1. Motivation

The fight against climate change requires tremendous effort that is characterized by the implementation of different solutions that must work and coexist together. Among the different renewable energy sources (e.g. wind, solar, marine energy), biomass is an important element in combating climate change and securing energy supply [11]. Today, biomass is already the largest source of renewable energy but, due to obsolete and inefficient exploiting methods and poor management strategies, its sustainability could be compromised. For example, traditional uses of biomass (e.i. combustion) are problematic, being highly inefficient and can expose people to harmful air pollutants [11]. However, biomass has great potential considered that it can be used to produce power, heat, cooling, liquid and gas fuels, thus providing a substantial alternative to fossil fuels. Sustainable biomass implementation is estimated to potentially contribute at 9 to 18% of total world energy supplies [11]. In addition, biomass utilization is forecasted to significantly increase in the next 15 years. Nevertheless, biomass is still today not globally implemented at the high level of sustainable capability needed for the energy transition [11].

Hence, it is important to keep developing and enhancing technologies for biomass exploitation. Gasification and torrefaction are two promising technologies for biomass implementation, whose knowledge is already relatively good. Nevertheless, huge steps can still be made to improve these processes and lead biomass to reach its full sustainable potential. This work therefore aims to gain more information regarding plasma gasification and gas-pressurized torrefaction, two novel technologies for biomass processing that still have to be comprehensively studied due to the nascent nature of the aforementioned technology.

1.2. Research Objectives

The purpose of this work is to compare and analyze different pathways for a thermochemical biomass-to-liquid (BtL) process for the production of liquid fuels. Two main modifications are brought to a base case BtL process model developed on Aspen Plus V12. They include the integration in the model of plasma gasification and GP torrefaction, and their effects are analyzed in detail, calculating key performance indicators (KPI).

1.3. Outline

An overview of the fundamentals of the subjects within this work is provided in Chapter 2. Therefore, a brief discussion on biomass is presented in Section 2.1, including topics on biomass compositions and sustainability. The following Section 2.2 focuses on torrefaction technology, furnishing insights regarding process mechanism, and GP torrefaction. In Section 2.3 the gasification process is described, highlighting the process reactions and parameters, with a final summary of plasma gasification technology. Then an overview of post-treatment processes for cleaning, conditioning and upgrading of the produced syngas from gasification is provided in Section 2.4, such as Acid Gas Removal (AGR), Water-Gas shift (WGS), wet-scrubbing and Fischer Tropsch Synthesis (FTS). Finally, the last Section (2.5) regards the state of the art of torrefaction and gasification studies.

In Chapter 3 the base case model (Section 3.1) and model modifications (Sections 3.2.2, 3.2.1) are described in detail, followed by the results presentation and discussion in Chapter 4.

2. Fundamentals and State of the art

In this chapter, a review of the fundamentals of the different sub-processes developed in the model are discussed. Therefore, some important aspects of torrefaction, gasification and post-treatment processes are described. Prior to this, summary of biomass is provided, whereas the final section of the chapter focuses on the state of the art of torrefaction and gasification

2.1. Biomass

As the world develops and countries to grow both economically and demographically, the energy demand increases all over the world, feeding the necessity for more and more energy. Moved by this driver and by the aggravation of the energy crisis, new technologies and energy sources are studied and progressively adopted. As stated by Azevedo et al. [8], biomass represents the largest and most important renewable energy option worldwide which can produce different forms of energy.

There are different treatments that the biomass can undergo. In the models presented in this work, torrefaction and gasification processes are employed and they are discussed in Sections 2.2 and 2.3. Liu et al. [39] described the effects of pre-treatment, treatment and post-treatment processes for the thermochemical conversion of Biomass.

Fuel Analysis and Composition

Biomass is a general term used to describe a complex heterogeneous mixture of organic matter and, to a lesser extent, inorganic matter with a wide range of chemical and phase compositions [69]. They vary considerably in terms of moisture and ash

content which gives them very different properties. For this reason, it is extremely important to define their chemical composition in order to investigate their potential application as energy fuels. Generally, the elements that can be found in biomass are: C, O, H, N, Ca, Na with higher abundance, Si, Mg, Al, S, Fe, P, Cl, Na in lower quantity and Mn, Ti as traces.

However, typical fuel analysis of biomass entails the proximate and ultimate analysis of said fuel. In the proximate analysis, moisture, ash, volatile matter and fixed carbon are all measured. Moisture content in biomass can vary between 3% and 63%, sometimes reaching 80%. It is a mineralized aqueous solution with charged and non-charged species with ash content having a wide range as well and it is formed mainly by the inorganic residue that results from the complete combustion (or oxidation) of biomass, while volatile matter typically includes hydrocarbons, CO, CO_2, H_2 and moisture.[69]. On the other hand, the ultimate analysis measures specific element yields (C, O, H, S, Cl, N) on a dry (db) or dry ash-free basis (daf), since the moisture and ash content strongly influence the characteristics of the biomass.

Sustainability

Sustainability is an important aspect of biomass. They are considered carbon neutral as they store CO_2 through the photosynthesis process and release it through combustion and other thermochemical or biochemical treatments. However, carbon neutrality can be achieved only with precise management of cultivation and treatment processes. As a matter of fact, as highlighted by Kircher [32], bio-based fuels and chemicals come with a carbon footprint that must be considered to include biomass in the sustainability discussion. This ac GHG emissions can be generated from cultivation methods as well as harvesting, storage and transportation.

Other critical aspects are discussed by Kudoh et al [34] who explained how the implementation of policies for the enhanced use of biomass can be related to loss of biodiversity, adverse impacts on communities' livelihoods, and increasing food insecurity [8], and to water security as well as deforestation (Popp et al [52]).

2.2. Torrefaction

One of the biggest advantages of biomass is the possibility to obtain not only liquid fuels but also power and chemicals through thermochemical or biochemical conversion. Liu et al. [40] gave a review of all thermochemical treatments and pre-treatments for biomass exploitation. It highlighted the importance of biomass pre-treatment to improve the conversion efficiency of the treatment process and reduce production costs. Torrefaction is a typical pre-treatment process aiming to improve biomass properties in order to obtain higher quality and attractive biofuels [68]. Indeed, there are some inconvenient properties of biomass such as a high moisture content as well as a high oxygen content that contributes to their low heating value. Therefore, torrefaction is employed to reduce the oxygen content in the biomass and to enhance its calorific value and energy density by decomposing the reactive hemicellulose fraction [68].

2.2.1. Torrefaction mechanism

Torrefaction is a low-temperature thermal conversion method for biomass operating in the absence of or drastically reduced amount of oxygen [18] and in the range between 200 °C and 300°C. It is typically used as a pre-treatment for gasification and co-firing. During the process of torrefaction, the biomass partly de-volatilizes leading to a decrease in mass, but the initial energy content of the torrefied biomass is mainly preserved in the solid product so the energy density of the biomass becomes higher than the original biomass which makes it more attractive for subsequent processes as well as transportation [68].

Complex kinetic models are used to describe the mechanism of torrefaction since several simultaneous reactions occur in the process. However, the treatment mainly involves hemicellulose decomposition that has high reactivity in the torrefaction temperature range, differently from cellulose and lignin which decompose at higher temperatures. The overall process can be divided into several steps:

- Initial heating: the biomass temperature increases but no relevant changes are observed.

- Pre-drying: once 100°C is reached free water starts to evaporate at constant temperature.
- Post-drying and intermediate heating: biomass temperature increases up to 200 °C and physically bound water escapes. Limited mass losses occur.
- Torrefaction: At the reaction temperature, hemicellulose decomposition begins followed by lignin and cellulose if higher temperatures are reached.

The temperature evolution deeply affects the process and the final output. Cremers et al. [18] stated that the higher the temperature or the longer the residence time the higher the torrefaction degree. More specifically, two torrefaction regimes can be identified. Light torrefaction undergoes below 240 °C, characterized by a predominant decomposition of hemiocellulose while cellulose and lignin are affected in much smaller amounts. On the other hand, severe torrefaction occurs above 270 °C and cellulose and lignin decomposition is more relevant [68].

Process layout

Torrefaction gases, obtained from the torrefaction of biomass contain a good amount of combustible gases (mainly CO) that can be burned to balance the heat duty and losses of torrefaction [15]. This is the case of autothermal operation. Others two cases exist. In the first case gases from the torrefaction do not contain enough energy to the process and an additional fuel is burned to meet the energy requirement of the process. On the other hand, the gas of torrefaction may contain more energy than is needed to balance the process. It means that the torrefaction was conducted under too extreme conditions leading to a loss of solid product [15].

However, torrefied gas combustion, together with an auxiliary fuel if needed, is usually actuated in order to generate heat and also for the drying of the biomass before entering the torrefaction reactor, which is part of the pre-treatment process. it is important to dry the biomass because it could result in a humid torrefaction gas, reducing its heating value, as well as reducing the process efficiency.

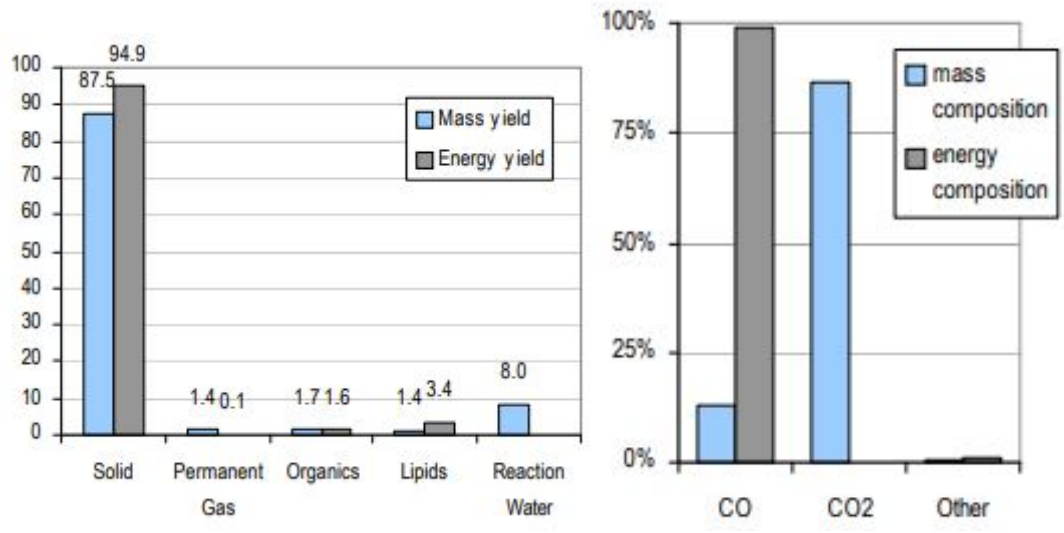

(a) Product groups yields (b) Gas composition

Figure 2.1.: Yield of product groups (a) and gas composition (b) [15]

Output products

The nature of the generated product during the torrefaction depends on its operation conditions and biomass properties. As reported in [15] they can be subdivided by their phase:

- The solid phase is formed mainly by char and ashes, but also original and modified sugar structures as well as new polymeric structures can be present.
- The liquid or condensed product can contain lipids and organics together with water in major quantities.
- Permanent gases are CO_2 and CO and traces of components as H_2 and CH_4

In figure 2.1, typical yields of the product groups are represented along with the compositions of the gases. Data are obtained from experiments conducted in [15]

2.2.2. Gas-pressurized torrefaction

GP torrefaction is conducted at high pressure with respect to the traditional torrefaction method which is performed at atmospheric pressure levels, resulting in a

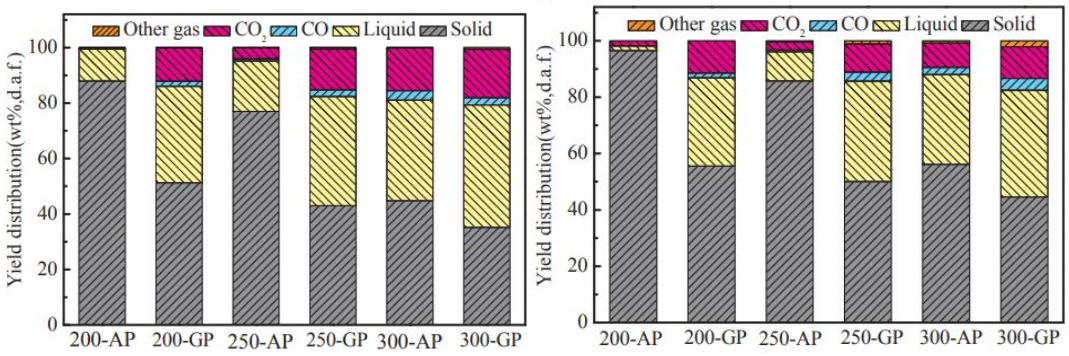

Figure 2.2.: Yield results of torrefied rice straw (a) and sawdust (b) at different temperatures in [65]

series of advantages. Tong et al. [65] analyze in detail the process by conducting an experiment with rice straw and pine sawdust, and compared the GP torrefaction with atmospheric pressure (AP) torrefaction. The two processes were performed at 250°C and 5 MPa for the GP torrefaction in a batch autoclave reactor. They claim that the torrefied product had a lower volatile matter and a higher carbon content due to enhanced aromatization reactions promoted by the higher pressure that converts part of the volatile matter into fixed carbon. Despite that, much higher CO_2 and CO yields were obtained with respect to AP torrefaction, particularly at 200°C as shown in Figure 2.2. The reason behind this is an increased decomposition of the hemicellulose and cellulose, which leads to a higher release of the two gases. Moreover, the oxygen content in the GP torrefied biomass was much lower than in the AP case which allowed to obtain a higher final heating value. Finally, they proved that the GP torrefied biomass had higher quality porosity and increased specific area, resulting in a better reactivity of the feed in the subsequent thermal conversion of said torrefied biomass [65].

2.3. Gasification

As already mentioned in Section 2.2, torrefaction is a pre-treatment process typically before the main biomass thermal conversion process, such as gasification. Gasification,

also known as "indirect combustion" is the conversion of biomass to synthesis gases through gasforming reactions occurring at temperatures between 700 °C and 1800°C [5][1]. It can be defined as a partial oxidation of the biomass in the presence of an oxidant amount lower than that required for the stoichiometric combustion [5]. In other words, the process partially involves combustion reactions that provide energy to gas-forming reactions, that are endothermic. Differently from combustion, gasification generates a hot fuel gas (named "producer gas" or "syngas") composed of partially oxidated products with a calorific value such as hydrogen, methane and carbon monoxide, rather than a hot flue gas as in the combustion [5].

To carry out the reactions, an oxidating medium is required. It affects the heat duty of the process and the calorific value of the final gas product, and it can be either air, oxygen-enriched air, pure oxygen, or steam. With this latter, no exothermic reactions are involved, therefore an external source of energy is required to continue the process [1]. It is the case of allothermal gasification, for example, plasma gasification (Section 2.3) where the energy is provided by a plasma torch. On the contrary, autothermal gasification gets the energy necessary for the endothermic reactions from the process itself, or rather from the partial combustion of the feed. For autothermal processes, air, oxygen-enriched air, or pure oxygen is used as the oxidizing medium. Air leads to a produced gas with a low calorific value due to atmospheric nitrogen that dilutes the syngas, while oxygen-enriched air and pure oxygen determine a relatively higher heating value.

Process steps

The main steps in the gasification process are heating, drying, de-volatilization and char reactions. Heating and drying take place up to 160 °C and involves liquid and steam migration from the porous solid phase [5]. De-volatilization (or pyrolysis) consists of the thermal cracking reactions at temperatures below 700 °C that release light gases, water vapors and tars, resulting in char production.

As volatiles and char are formed, they start reacting with oxygen through semi-oxidation 2.1 and combustions 2.2 reactions that provide energy for the other reactions

and steps, assuming an auto-thermal process.

$$C + \frac{1}{2} O_2 \longrightarrow CO \tag{2.1}$$

$$C + O_2 \longrightarrow CO_2 \tag{2.2}$$

The other gas-forming reactions are listed in Table 2.1.

Table 2.1.: Gas-forming reactions during gasification

Reaction	Reaction Enthalpy	Name
$C + H_2O \longleftrightarrow CO + H_{20}$	(+131.3 kJ/mol)	water-gas
$C + 2\,H_2O \longleftrightarrow CO_2 + 2\,H_2$	(+90.2 kJ/mol)	carbon-steam
$C + CO_2 \longleftrightarrow 2\,CO$	(+172.4 kJ/mol)	Boudouard
$C + 2\,H_2 \longleftrightarrow CH_4$	(-75 kJ/mol)	hydrogasification
$CO + H_2O \longleftrightarrow CO_2 + H_2$	(-41.1 kJ/mol)	water-gas shift
$CO + 3\,H_2 \longleftrightarrow CH_4 + H_2O$	(-206.1 kJ/mol)	methanation
$CO + \frac{1}{2} O_2 \longleftrightarrow CO_2$	(-283 kJ/mol)	carbon monoxide oxidation
$H_2 + \frac{1}{2} O_2 \longleftrightarrow H_2O$	(-242 kJ/mol)	hydrogen
$CH_4 + \frac{1}{2} O_2 \longleftrightarrow CO + 2\,H_2$	(-38 kJ/mol)	methanation

Moreover, the high temperature facilitates the tar cracking in gas components as indicated by reactions in Table 2.2.

Table 2.2.: Tar-cracking reactions

Reaction	Reaction Enthalpy	Name
$C_mH_n + \frac{m}{2} O_2 \longleftrightarrow \frac{n}{2} H_2 + m\,CO$	(+131.3 kJ/mol)	partial oxidation
$C_mH_n + m\,CO \longrightarrow \frac{n}{2} H_2 + 2\,m\,CO$	(+90.2 kJ/mol)	dry reforming
$C_mH_n + m\,H_2O \longrightarrow \left(m + \frac{n}{2}\right) H_2 + m\,CO$	(+172.4 kJ/mol)	Stream reforming
$(m - p)\,C_mH_n \longrightarrow m\,C_{m-p}\,H_{n-q} + \frac{mq-pn}{2} H_2$	(-75 kJ/mol)	thermal cracking

Process parameters

A series of key parameters is important to define the gasification process and assess its performance. They are deeply explained in [5] and are reported here:

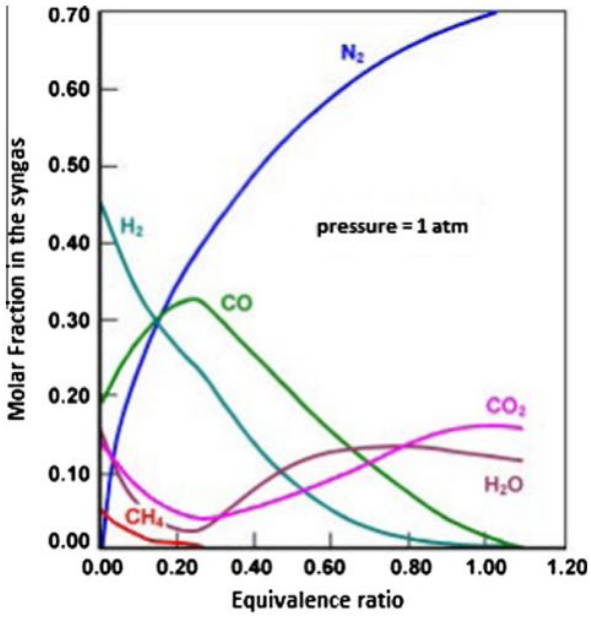

Figure 2.3.: Syngas molar fraction dependence on equivalence ratio

- *Equivalance ratio* (E/R). The ratio of oxygen content in the oxidant agent to stoichiometric oxygen required for a complete combustion. It can affect the gas composition and therefore heating value too. In Figure 2.3, the dependence of syngas components molar fraction on the equivalence ratio is represented. Values between 0.25 and 0.35 seem to maximize char conversion even though it can be increased up to 0.5. Values too low could lead to unconverted char and a higher amount of tar, while partial oxidation of syngas can occur with too high values.

- *Reactor temperature*: It can influence the state of ashes and tar content in the syngas.

- *Residence time*: It is defined by reactor type and design.

- *Biomass composition and physical properties*: They significantly affect the process and its performance. Pre-treatment solutions are used to obtain a more suitable fuel for the gasification, as already discussed in Section 2.2.

- *Composition of the gasifying medium*: It affects the mass and energy balance of the

process.

- *Cold Gas efficiency*: Describe the efficiency of the conversion process without considering the sensible heat of product and feed. It is calculated as :

$$CGE = \frac{m_{syngas}\ LHV_{gas}}{m_{feed}\ LHV_{feed}} \tag{2.3}$$

- *Hot gas efficiency* expresses the same concept of CGE, but takes into consideration the sensible heats of the streams:

$$HGE = \frac{m_{syngas}\ LHV_{gas} + H_{syngas}}{m_{feed}\ LHV_{feed} + H_{feed}} \tag{2.4}$$

- *Carbon Conversion efficiency* keeps track of the amount of converted carbon into the new energy carrier. It is calculated

$$CCE = \frac{m_{syngas}\ C_{gas}}{m_{feed}\ C_{feed}} \tag{2.5}$$

  with C being the carbon fraction in the feed or syngas.

- *Tar content*: Tar is a subproduct of gasification that can cause serious problems to the conversion system and end-use devices. It is therefore important to estimate its yield.

Plasma Gasification

As already mentioned above, plasma gasification is an allothermal conversion process in which a plasma torch is employed to provide energy for gasification. With respect to the conventional treatment, plasma gasification occurs at a much higher temperature, up to 5000 °C [23]. This brings some advantageous features for the conversion of biomass. Firstly, the process can be carried out efficiently with a wider range of feedstock resulting in enhanced flexibility. Secondly, since the energy is externally imported, combustion and oxidation reactions play a second role in the process. Therefore, the oxidant medium is not needed as in the case of conventional processes. In addition, the CO_2 content normally generated from combustion is significantly reduced in the syngas. The same is true for the tar generation, which is drastically

reduced since the tar cracking is highly promoted by the extremely high temperature. For these reasons, the produced syngas has a much higher quality than the one obtained by traditional gasification, with an increased heating value [23]. However, such high operation temperatures require a great amount of energy that increases the economic costs and reduces the overall efficiency of the process.

Beyond these advantages, plasma gasification can be controlled relatively easily compared to the traditional one due to the fact that the energy input from combustion reactions is less precise, and the energy transfer from the plasma torch to the feedstock is more efficient [23].

2.4. Post-treatment processes

Syngas is the main product of the gasification, a mixture of hydrogen, carbon monoxide, CO_2 and other gases. Depending on its use, which can be power production, fuels and chemical synthesis, it must be treated in order to mitigate the contaminants and meet the process requirements and pollution control regulations [71]. Indeed, raw syngas contain a relatively high amount of impurities that can affect and seriously damage the downstream applications [71]. In particular, sulfur, nitrogen and chloride can interfere with other gas components and generate impurities that have specific damaging effects on downstream components and processes. It is therefore important to select the suitable port-treatment process. For example, for power generation application of syngas, CO_2 does not represent a problem since there are no chemical reactions involved and only the latent heat of syngas is converted [46]. Contrarily, in other applications such as the synthesis of fuel or chemicals, there is a specific threshold of CO_2 admitted, hence a separation process is required. In table 2.3 the requirements in terms of amounts of CO CO_2 and Sulfur for the treated syngas in different applications are described.

Contaminants

Contaminant yields in the syngas are highly influenced by feedstock nature and composition. However, the polluting elements that are mostly present in the product

Table 2.3.: Desired quality of treated syngas for downstream applications [46]

Syngas comp.	**Power**	**Hydro-processing**	Chemical
Sulfur (wppm)	10-15	<1	<0.01-1
CO_2 (vol%)	-	<0.1	0.05-2.0
CO	-	<50 wppm	H2/CO control as per requirement

syngas are:

- *Particualte matter*. It mainly derives from inorganic compounds in the biomass and residual solid carbon from its gasification. Fouling and corrosion can occur if particulate matter is present in the syngas which can lead to decreased efficiency and safety issues. For these reasons, a 99% particulate matter removal is often required.

- *Tars*. Tars are condensed organic compounds that can be highly harmful to system components. Different operational parameters generate a wide range of tars species with very complex chemical compositions that make them difficult to analyze and define. Generally, they are defined as "all hydrocarbons with molecular weights higher than that of benzene. They are conventionally classified into primary, secondary and tertiary tars [71], whose formation depends on temperature and residence time. Lower temperatures and shorter residence time generate primary tars, which come from the devolatilization of biomass, mainly formed by organic compounds. Whether temperature and/or residence time are increased, tars decomposition is enhanced resulting in reduced tars yields with higher weight. In this way, secondary and tertiary tars are generated which are formed by phenolics and olefins in the first case and polycyclic aromatic hydrocarbons in the latter case. If not removed, tars can create fouling and clogging in pipes, filters and engines. More problematic is the deactivation of catalysts in electrolyzers.

- *Sulphur* Sulfur pollutants cause problems such as metal surface corrosion, but also catalyst poisoning. They are present as hydrogen sulfide H_2S as well as carbonyl sulfide COS and SO_2 to a lesser extent [71]. This latter is generated

from H_2S if oxygen is present.

- *Nitrogen compounds* Mostly ammonia NH_3 with smaller quantity of hydrogen cyanide HCN. NH_3 can be either formed directly from biomass or from secondary reactions with HCN. Ideally, N_2 is the main product of equilibrium as long as enough temperature and residence time is provided. However, in practice, nitrogen component yields and NH_3 yields increase with temperature while H_2 availability and residence time encourage conversion from HCN to NH_3. [71]

- *Chlorides* They are the most abundant pollutant in the syngas mainly in the form of HCl. Reactions can also occur between HCl and other contaminant species in the gas phase, which creates more compounds such as ammonium chloride (NH4Cl) and sodium chloride (NaCl) [71]. The associated problems are fouling, deposits and catalyst poisoning.

2.4.1. Gas cleaning and conditioning

As already mentioned, to avoid a severe problem in downward components, post-treatment processes must be actuated to clean and condition the produced syngas. Wet scrubbing, WGS and AGR are some possible treatments and are employed in the model discussed in Section 3.

Wet scrubbing

The term "wet" is used to describe a cleanup treatment at low temperatures. It is a simple and effective process, widely used in industry that aims to remove pollutants such as particulate matter, chlorides, and nitrogen compounds. However, the relatively low operational temperatures affect the overall efficiency of the biomass process since the sensible heat of the produced gas is lost. The general concept behind this technology is to put in contact the dirty gas with the scrubbing liquid (i.e. water) that absorbs soluble gas contaminants. Different designs with different operating principles exist. A spray scrubber is the most basic design, with spray nozzles that disperse the liquid into a concurrently or counter-currently flowing gas stream [71].

Water-Gas shift

Water-gas shift treatment does not aim to remove a pollutant element from the syngas. However, the syngas produced by the gasification contains high amounts of CO, which is not desirable for many downstream applications [46]. Hence, proper treatment is used to avoid related problems. The treatment aims to convert CO in H_2 and CO_2 reacting with H_2O, as in accordance with the water-gas shift reaction:

$$CO + H_2O \longrightarrow H_2 + CO_2 \qquad \Delta H = -41.1 kJ/mol \tag{2.6}$$

Following the thermodynamics of the shift reaction, the conversion of CO to H2 is favored at higher temperatures, which allows recovery of the heat of the reaction at sufficiently high levels to generate high-pressure (HP) steam [46]. Two cases can be distinguished: a sweet-gas shift if the WGS occurs after the AGR and a sour-gas shift reaction in the opposite case. They slightly differ in performance and operation. In the first case, two high-temperature and one low-temperature conversion steps are included resulting in a CO concentration reduction from 44.6% to 0.5%. On the other hand the conversion in the the latter case goes from 44.6% to 1.8%, involving two or three conversion stages and more steam usage with respect to sweet-gas shift which is not economically beneficial.

Acid Gas Removal

Acid gas removal is a treatment suited for CO_2 and H_2S. Different methods of removal exist which are grouped into wet and warm processes. Wet processes use different types of solvents and are based on physical absorption and chemical absorption or a combination of the two. In chemical absorption processes, acid gas components react with solvent molecules and dissolve in the solvent [46], while in physical absorption processes, syngas components are physically absorbed into the solvent molecule [46]. The most diffused processes are the Selexol process, which employs polyethylene glycol and Rectisol process which employs refrigerated methanol. In both chemical and physical processes, once the absorption is completed H_2S is desorbed at high temperature and recovered through the Claus process. On the contrary, warm processes are based on adsorption. They use adsorbents such

as ZnO/CuO and Cr_2O_3 that react with H_2S at temperatures between 315 and 530 °C [46]. Another reaction of oxidation in the temperature range 590-680 °C returns regenerated ZnO and SO_2 (reactions 2.7, 2.8) [46].

$$ZnO + H_2S \longrightarrow ZnS + H_2O \tag{2.7}$$

$$ZnS + \frac{3}{2} O_2 \longrightarrow ZnO + SO_2 \tag{2.8}$$

The same adsorbent works also for CO_2 adsorption.

2.4.2. Fischer- Tropsch Synthesis

Once the syngas undergoes the due treatment of conditioning and cleanup, it is ready to be used in the FTS. The FTS is a surface polymerization reaction in which the reaction between the reagents, hydrogen and carbon monoxide takes place on the surface of the catalyst [41]. Despite the FTS is still nowadays not a well-understood process, different mechanisms were proposed to govern the composition of the output product of the synthesis. In general, reagents (CO and H_2) form monomer units which are the starting point for the polymerization process leading to the production of several hydrocarbons with chain lengths from C_1 to C_{40}.

Mechanism

Throughout the overall process, a series of reactions occur simultaneously.

$$nCO + (2n + 1) H_2 \longrightarrow C_nH_{2n+2} + nH_2O \tag{2.9}$$

$$nCO + 2\ {}_nH_2 \longrightarrow C_nH_{2n} + nH_2O \tag{2.10}$$

$$C_nH_{2n} + H_2O \longrightarrow C_nH_{2n+2}O \tag{2.11}$$

Reactions 2.9 and 2.10 describe the formation of paraffins and olefins respectively, which are the main product of the FTS, while reaction 2.11 regards the formation of alcohol. This latter can be a by-product whose quantity is determined by the type of catalyst and pressure [36]. Mahmoudi et al. also claimed the possibility of alcohol and other oxygenated products generation through reactions 2.12 and 2.13 as well as

WGS reaction dependent on the catalyst as discussed in [41] and [3]

$$\mathrm{nCO} + 2\,n\,\mathrm{H_2} \longrightarrow \mathrm{H(CH_2)}_n\mathrm{OH} + (\mathrm{n\text{-}1})\,\mathrm{H_2O} \tag{2.12}$$

$$\mathrm{nCo} + (2\,\mathrm{n\text{-}1})\,\mathrm{H_2} \longrightarrow (\mathrm{CH_2})_n\mathrm{O} + (\mathrm{n\text{-}1})\,\mathrm{H_2O} \tag{2.13}$$

The process is highly dependent on reactor temperature, pressure, H_2/CO ratio in the syngas and type of catalyst, which affect the final composition of the product mix. In particular, relatively low pressure, between 473 and 513 K leads to abundant high molecular weight waxes in the syncrude, rather than lower molecular weight components such as ethylene and propylene at 573-623 K. In other words, the higher the temperature the higher the amount of light product. Therefore, since the (FT) reactions are strongly exothermic, effective heat removal from the reactor is necessary, in order to prevent elevated yields of light gaseous hydrocarbons. Furthermore, in worst-case scenarios, high temperatures can deactivate the catalyst as a consequence of coking, sintering, or catalyst disintegration [36].

Catalysts

Catalysts are a fundamental element for the FTS. Generally, the most active metals for the FTS are iron, cobalt and ruthenium. However, this last one is excluded from industrial applications for its high cost and low availability, even though it is the most active. The choice of the catalyst must be carefully studied depending on the desired application and output product of the FTS. For instance, iron catalysts promote WGS reactions and the selectivity of high molecular weight hydrocarbons[41].

Iron catalysts consist of precipitated iron, promoted with copper and potassium obtaining a high activity and selectivity [36]. In addition, silica is usually added as a binder to improve the rigidity of the catalyst [41]. In cobalt catalysts, Cobalt nanoparticles are usually dispersed on carriers such as metal oxides, zeolites, carbon material and silicon carbide, in order to increase the exposure of atoms and reduce the cost [41] [36].

2.5. State of the art

With the continuous aggravation of the climate crisis, the need for alternative energy sources led, and still leads nowadays the research to the development of new or already existing renewable sources. This resulted in an increased interest in biomass and its treatment process such as torrefaction and gasification. Gasification has been already deeply studied for both coal [13, 38, 17, 70, 44, 45, 31] biomass [55, 56, 2, 63, 58, 42] exploitment. For torrefaction, on the other side, a large number of scientific literature is also present but represents only 3% compared to gasification in terms of scientific literature. Van der Stelt et al. [15] provided an overview of the research on biomass upgrading by torrefaction, describing its characteristics and history. Another comprehensive review was given by Tumuluru et al. [67], detailly including product properties, off-gas composition and methods used. However, there are much fewer documents when it comes to plasma gasification and even fewer for pressurized torrefaction.

Plasma gasification

The plasma gasification process was analyzed by Rajasekhar et al. [54] and Saleem et al. [57] for municipal solid waste and biomass respectively. Saleem et al. also studied the effect of carrier gas such as N_2, H_2, CO_2, CO on the output products and decomposition of tar analog (toluene). It was shown how CO allows the maximum decomposition of toluene with 89.1% of removal. Studies with different feedstocks are also carried out by Janajreh et al. [30], who developed two methods for plasma gasification and conventional air gasification to be compared. In the first case, air/steam is used as an oxidizer, while only air is used in the second case. The results show that plasma gasification achieved high efficiency even with different feedstock. Similar conclusions were obtained by Pang et al. [48]claiming that plasma-assisted gasification enhances the flexibility of the process as well as the reaction kinetics. A plasma gasification process model was developed and thermodynamically analyzed with Aspen Plus by Aneke et al. [4]. They showed that plasma technology reduces the tar content in the syngas with an increased heating value but with a high electrical energy cost due to the electricity requirement to generate plasma. The result was

37.3% overall process efficiency compared to 43.6% for the conventional case. Two other process models were developed by Kuo et al. [35] and Mazzoni et al. [43]. In Kuo et al. work, three different gasifying agents (air, steam and CO_2) were used to study the plasma gasification of raw and torrefied woody, non-woody and algal biomass. They studied the impact of feedstock and gasifying agents on the various performance indices. They also calculated plasma energy to syngas production energy (PSR) and plasma gasification energy (PGE) obtaining the lowest PSR and highest PGE with CO_2 as a gasifying agent. In the other case, Mazzoni et al. simulated and compared the behavior of a plasma gasification process with a traditional entrained flow gasification. The results showed how plasma gasification has better Cold Gas Efficiency (CGE) compared to the conventional one, with 74.8% and 71.6% CGE, respectively. Some other scientific documents were found regarding plasma gasification models. However, most of them were about numerical or mathematical models [27, 29, 28, 25]and none of them included process modeling. This shows a lack of literature on plasma gasification process modeling.

Gas-pressurized torrefaction

A lot of scientific documents can be found regarding conventional torrefaction [53, 50, 22, 61, 16, 67, 14]. Nevertheless, literature on gas-pressurized torrefaction is very limited. The major part of it studies the effects of pressure on the process comparing them with conventional torrefaction at atmospheric pressure (AP) [19, 66, 20, 37, 64, 60, 65, 26, 72, 62]. In 2023, Shi et al. [60] tested the deoxygenation in lignocellulosic solid waste for gas-pressurized (GP) and atmospheric torrefaction, with a 79% and 40% oxygen removal respectively. In addition, results demonstrated that gas pressure promoted 90.4% of cellulose composition and the conversion of volatile matter to fixed carbon. Similar outcomes were obtained by Tong et al. [66] and Tan et al. indicating that GP torrefied biomass had higher carbon content and lower volatile matter compared to AP. Better products in terms of weight losses, heating value, ash content, O/C ratio and H/C ratio were found by Huang et al. [26], while an increased activation energy of the torrefied biomass in the range 195 to 198 $kJmol^{-}1$ was obtained by Dacres et al. [19]. Tan et al. [64] studied the effects of temperature, carrier gas composition and reactor type on torrefaction product as well, compared

to AP.

Few articles on torrefaction modeling were found, but none of them included GP torrefaction. In [9, 51, 49, 10, 24, 47] works process models for conventional torrefaction are developed while in [12, 59, 33] the kinetic is modeled. This shows a clear lack of literature on process modeling for gas-pressurized torrefaction.

3. Models

In this work, two models are developed using Aspen Plus V12.0. Both of them simulate the pretreatment processes of biomass and intermediate products for the production of different final products. The process includes seven different sections: pretreatment, gasification, quenching, water gas shift, acid gas removal, Fisher-Tropsch synthesis, and upgrading.

The base case model is based on Marcel Dossow's [21] model and it is described in details in Section 3.1. In Section 3.2, a similar model is presented, which features some modifications from the base model.

3.1. Base case simulation model

The base case model main flowsheet is shown in Figure 3.1.

It simulates a biomass treatment process for the production of biofuels such as jet fuels, gas-oil, and other synthetic products derived from biomass. To model the process, seven hierarchy blocks are involved to include the subsystems of the respective sections: PRETREAT(Pretreatment), GASIFIC(gasification), QUENCH (quenching), WGS (water-gas shift), AGR (acid gas removal), FTS (Ficher-Tropsch synthesis), UPGRADE (fuel upgrade). In addition, a stream class changer block (CHANGER) is connected between QUENCH and WGS blocks. Its utility is to change the stream class of the first part of the flowsheet (MCINCPSD) in CONVEN stream class for the latest sections of the framework.

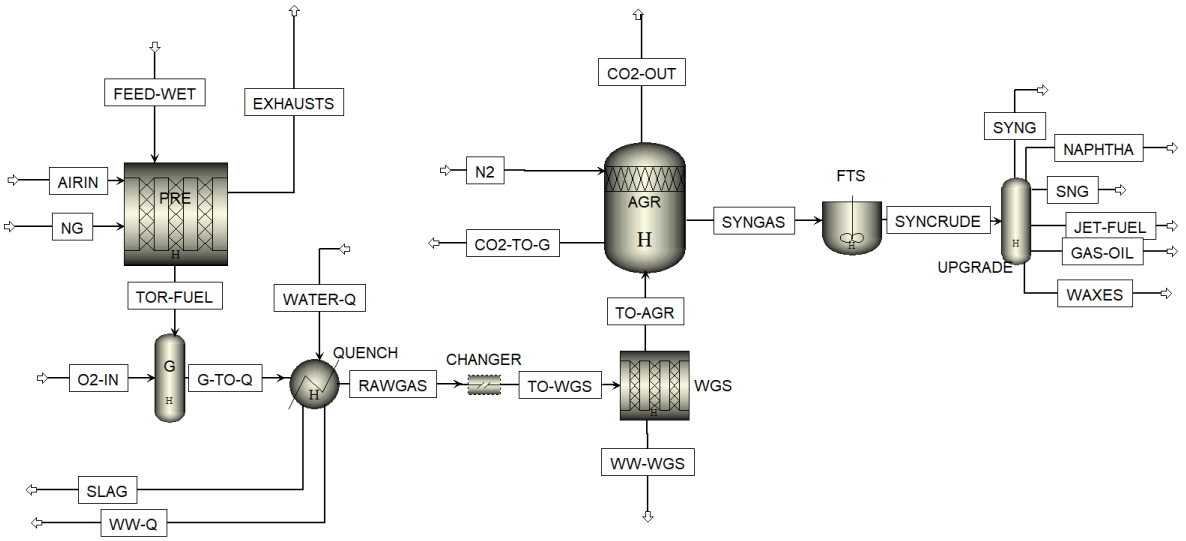

Figure 3.1.: Main Simulation flowsheet

3.1.1. Preliminary Setup

The global section represents the higher level of the hierarchy. Thus, every specification made for this section is valid for lower levels.

Properties environment setup

Before starting, a proper property setup is necessary for the correct functioning of the model. This includes methods, components, and chemistry in the property environment of Aspen Plus.

Property Method Property methods in Aspen Plus define the manner in which the physical and chemical properties are calculated. Its choice is important for the correct functioning of the model. The Peng-Robinson equation with Boston-Mathias modifications (PR-BM) is selected to estimate the properties of available conventional components in liquid and gas phases and non-conventional components property [21]. Also, again in the method specification sheet, the free-water method is set as STEAMNBS. This method calculates thermodynamic properties for systems containing pure water or steam and allows for the convergence problems and wrong trends due to boundary continuity to overcome [6].

Components In the component sheet, all components involved in the simulation are declared and are listed in Table A.1 with the respective information. Particular attention must be placed on MIS, BEECH, TORMIS, TORBECH and ASH components since they are declared as non-conventional components. MIS, BEECH represent the biomass feedstock which is a mixture of miscanthus and beech wood, TORMIS, TORBECH their respective torrefied product. Thus, in the `Methods\NC Props\Property methods folder`, the method used to calculate the nonconventional solid properties is specified. This is because they are heterogeneous solids that do not participate in chemical or phase equilibrium, hence specific methods must be adopted. For each non-conventional component in the enthalpy field, HCOALGEN is selected, which automatically includes PROXANAL, ULTANAL, and SULFANAL in the Required component attributes field [7]. This allows for the proximate, ultimate, and sulfate analyses to be defined in the simulation environment during the modeling phase. Then, the first option code must be changed from 1 to 6 to allow heat of combustion calculations. The heat of combustion (HCOMB) represents Higher Heating Value (HHV). It is accessed by creating a new pure component parameter in the `Parameter\Pure component` folder. For MIS and BEECH, a value of 12.7 MJ/kg_{dry} and 17.5 respectively is defined on a dry basis, in accordance with the fuel analysis, while a placeholder value, that will be overwritten throughout the simulation, is assigned for TORMIS, TORBECH. In the density field instead, DCOALIGT is selected.

Chemistry For the quench section (3.1.4), a set of equilibrium reactions is specified in the chemistry sheet of the properties environment (3.1). Also, CO_2, H_2S, Cl_2, HClO, SO_2, NH_3, HCN, HCl, H_2, O_2 and N_2 are indicated as Henry's components.

Simulation environment Setup

In the simulation environment, it is necessary to specify the stream classes that will be used in the model as well as the Particle Size Distribution (PSD)

Stream Classes Since some of the components in the model are non-conventional, those streams that contain them must be declared as MCINCPSD which is used for models with both conventional and non-conventional components. Therefore, in the

Table 3.1.: Equilibrium reactions for quench modeling

$NH_3 + H_2O \longleftrightarrow NH_4^- H^-$
$H_2O + HCLO \longleftrightarrow CLO^- + H_3O^+$
$2\,H_2O + CL_2 \longleftrightarrow HCLO + CL^- + H_3O^+$
$HCN + H_2O \longleftrightarrow CN^- + H_3O^+$
$H_2O + HSO_3^- \longleftrightarrow H_3O^+ + SO_3^{--}$
$2\,H_2O + SO_2 \longleftrightarrow H_3O^+ + HSO_3^-$
$HCL + H_2O \longleftrightarrow CL^- + H_3O^+$
$NH_3 + HCO_3^- \longleftrightarrow H_2O + NH_2COO^-$
$H_2O + HCO_3^- \longleftrightarrow CO_3^{--} + H_3O^+$
$2\,H_2O + CO_2 \longleftrightarrow HCO_3^- + H_3O^+$
$HS^- + H_2O \longleftrightarrow H_3O^+ + S^{--}$
$H_2S + H_2O \longleftrightarrow H_3O^+ + HS^-$
$2\,H_2O \longleftrightarrow H_3O^+ + OH^-$

stream class sheet, two sections for the model are created. One with MCINCPSD stream class for the first part of the flowsheet (PRETREAT, GASIFIC, QUENCH and CHANGER blocks) and one with CONVEN stream class for the remaining blocks. MCINCPSD allows for the selection of MIXED, NCPSD and CIPSD substreams. MIXED handles components that participate in phase equilibrium whenever flash calculations are performed and can have liquid and vapor phases. NCPSD handles non-conventional solids that have no defined molecular weight with PSD, while CIPSD is used for homogeneous solids that have a defined molecular weight with PSD information [7]. CONVEN has only MIXED as substream.

PSD Particle Size Distribution is requested in the solid folder as NCPSD components are present. A PSD of 13 intervals is assumed with 10 regular sections of 20 μm up to 200 μm and further sections from 200 to 300, 300 to 700, and 700 to 16000 microns [21].

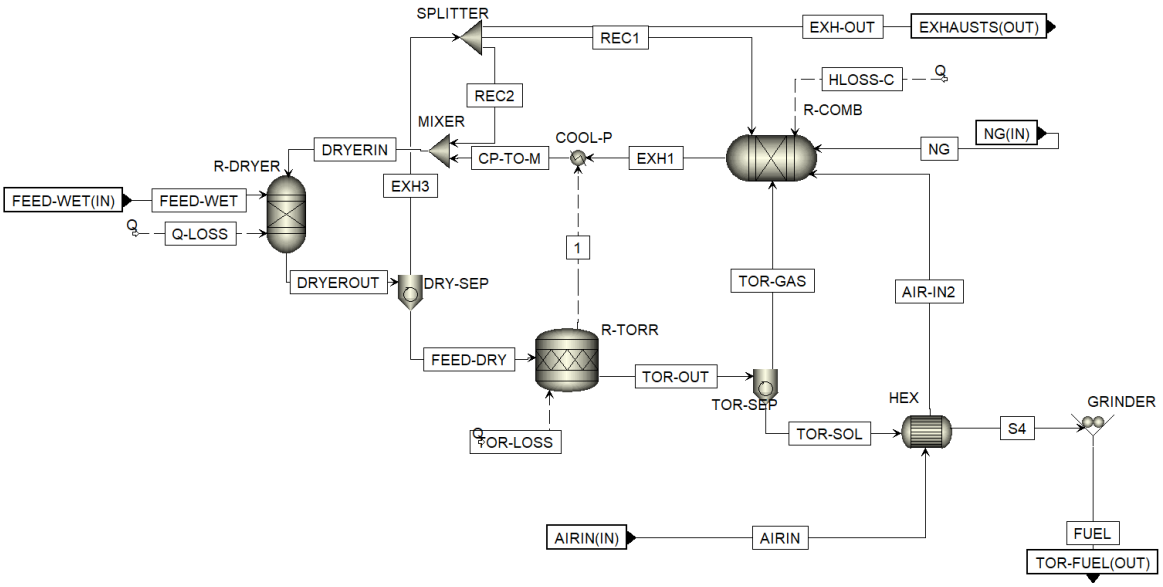

Figure 3.2.: Pretreatment Flowsheet

3.1.2. Pretreatment

The pretreatment flowsheet (Figure 3.2) is developed in the respective hierarchy block PRETREAT and models the drying and torrefaction processes of the biomass. The implemented blocks are described in Table A.2 in the appendix. Totally, three RStoic reactors are used, a heater block, two Cyclon blocks, an FSplit, a Mixer, a HeatX block and a Crusher.

Pretreatment flowsheet Description

The drying of the biomass is performed by the R-DRYER block which is fed by the FEED-WET stream. The biomass enters with a mass flow rate of 5538,46 kg/h at a temperature of 25°C and 1 bar, as specified on the stream NC-Solid specification sheet. Here, it is necessary to define the values of the proximate and ultimate analysis as weight percentages on a dry basis (Table A.7 in the appendix). The data are provided from experimental tests by the Chair of Energy Systems of the Technical University of Munich (TUM). The wet biomass has a starting moisture of 30 wt% and is dried by the air and exhausted gasses of the methane combustion in the R-COMB

stoichiometric reactor. The R-DRYER block implements reactions 3.1 and 3.2:

$$MIS \longrightarrow \gamma\, H_2O \tag{3.1}$$

$$BEECH \longrightarrow \gamma\, H_2O \tag{3.2}$$

$$\tag{3.3}$$

where γ is calculated as $\gamma = 1/MW_{H_2O}$, with MW_{H_2o} being the molar weight of water since Aspen Plus treats all non-conventional components as if they have a molecular weight of 1. The fractional conversion of the biomass is calculated in the C-DRYER calculator block (3.1.2). Another calculator block (C-QLOSS) estimates the heat losses in the dryer modeled by heat stream Q-LOSS.

At the outlet of the dryer block, the biomass exits with 10 wt% of moisture, so it is specified in the components attribute sheet of the R-DRYER. However, its proximal and ultimate analyses do not change since their values are dry-based. The temperature is set at 80°C by the design specification NG-IN. Then, the biomass is separated from the exhaust gasses by means of DRY-SEP. The exhaust gasses are partially recirculated through REC1 and REC2 in order to control the temperatures of EXH1 and DRYERIN streams. To do this, a FSplitter (SPLITTER) and a Mixer (MIXER) are used together with a design specification that sets the split fraction of SPLITTER to meet the requirement of 200°C for DRYERIN stream.

After this, the dried biomass reaches the torrefaction reactor. Its thermal requirement is supplied by the combustion exhausts through COOL-P, and TOR-LOSS represents heat losses calculated in Q-LOSS. What is obtained are volatile subproducts (reactions from 3.5 to 3.12) and a torrefied biomass with compositions defined in Table A.7.

$$MIS \longrightarrow TORMIS \tag{3.4}$$

$$MIS \longrightarrow \gamma_{H2O}\, H_2O \tag{3.5}$$

$$MIS \longrightarrow \gamma_{CO}\, CO \tag{3.6}$$

$$MIS \longrightarrow \gamma_{CO2}\, CO_2 \tag{3.7}$$

$$\tag{3.8}$$

$$BEECH \longrightarrow TORBEECH \tag{3.9}$$

$$BEECH \longrightarrow \gamma_{H2O}\, H_2O \tag{3.10}$$

$$BEECH \longrightarrow \gamma_{CO}\, CO \tag{3.11}$$

$$BEECH \longrightarrow \gamma_{CO2}\, CO_2 \tag{3.12}$$

TORMIS and TORBECH are the torrefied biomass products and γ_i are the reaction coefficient, calculated as the inverse of the molar weight of each substance. Calculator block TORCALC is used to calculate the fractional conversion of biomass for each reaction and HHV of the torrefied product.

In the following block (TOR-SEP), TORMIS and TORBECH are separated from the volatiles which are fed to the R-COMB block. Here, the volatiles combusted with CH_4 in order to heat the air necessary for the biomass drying. 137 kg/h of CH_4 are provided to the reactor by NG stream, depending on a dedicated design specification NG-IN that adjusts its mass flow to meet a temperature of 80°C at the outlet of the dryer. In addition, the air entering the combustor is pre-heated in the HEX heat exchanger with heat at 250°C from the torrefied biomass. To achieve a temperature of 35°C of the cooled torrefied biomass, the design specification AIR-IN determines the mass flow rate of AIRIN and sets it at 8300 kg/h. Since the purpose of this stream is to represent air, it is specified as a mixture of CO_2, N_2 and O_2 with respective mass fractions of 0,0004, 0,7897 and 0,2099.

Finally, the cooled torrefied product enters the GRINDER and it is broken into particles with a maximum diameter of 300 μm. What is obtained is an optimized final product that will enhance gasification performance.

Pretreatment Calculations

A set of equations are implemented as Fortran statements in the calculator block to calculate the model's necessary parameters. For the pretreatment section, 4 calculators are created: C-DRYER, Q-LOSS, TORCALC and C-PRE

C-DRYER It is used to calculate the fractional conversion of the reaction 3.1 and 3.2 with equation 3.13 and 3.14 [21]. After the calculation, the placeholder value in the

R-DRYER is substituted with the new value.

$$X_{MIS} = \frac{\frac{\nu_{in}}{100} - \frac{\nu_{out}}{100}}{1 - \frac{\nu_{out}}{100}} \tag{3.13}$$

$$X_{BEECH} = \frac{\frac{\nu_{in}}{100} - \frac{\nu_{out}}{100}}{1 - \frac{\nu_{out}}{100}} \tag{3.14}$$

ν_{in} and ν_{out} are the moisture contents in % in the biomass at the inlet and outlet of the dryer respectively.

Q-LOSS In this block, heat losses of the three RStoic reactors are estimated. Equations 3.15, 3.16, 3.17 return their results to Q-LOSS, TOR-LOSS, HLOSS-C streams heat duty in kJ/s. They are defined as the percentage of HHV of the inlet stream of each reactor, multiplied by their mass flow rate.

$$\dot{Q}_{L,Dryer} = -0.005 \cdot \dot{m}_{wetbio} \cdot HHV_{wetbio} \tag{3.15}$$

$$\dot{Q}_{L,Torr} = -0.005 \cdot \dot{m}_{drybio} \cdot HHV_{drybio} \tag{3.16}$$

$$\dot{Q}_{L,Comb} = -0.01 \cdot \dot{m}_{\mathrm{CH_4}} \cdot HHV_{\mathrm{CH_4}} \tag{3.17}$$

$\dot{m}_{wetbio}$, $\dot{m}_{drybio}$, and $\dot{m}_{\mathrm{CH_4}}$ are the mass flow rates in kg/s of the inlet streams of the three reactors, and HHV_i the corresponding higher heating values. In the R-DRYER, enters wet biomass, dry biomass in R-TORR and CH_4 in R-COMB, respectively. Also, the minus sign in front of each expression defines the exiting direction of the heat fluxes [kJ/s] from the reactors.

TORCALC Firstly, the fractional conversions of biomass for torrefaction reactions (3.4-3.12) are calculated. For the conversion into the torrefied product (reaction 3.4), equation 3.18 [21] is used, where T_{torr} is the torrefied temperature at 250°C.

$$X_{biomass}^{DAF} = \left.\frac{m_{torr,solid}}{m_{biom}}\right|_{DAF} = -5.645 \times 10^{-5} \cdot T_{torr}^2 + 0.0239 \cdot T_{torr} - 1.5789 \tag{3.18}$$

Since the results are on a Dry Ash Free (DAF) basis, it must be converted on a wet basis as the components MIS and BEECH in the reactions have 10% of humidity.

$X^{DAF}_{biomass}$ refers to the fractional conversions of both miscanthus and beechwood.

$$X^{WET}_{tor,mis} = X^{DAF}_{mismiscanthus} \frac{(1-\nu_{bio}) \cdot (1-\phi_{bio})}{(1-\nu_{tormis}) \cdot (1-\phi_{tormis})} \tag{3.19}$$

$$X^{WET}_{tor,beech} = X^{DAF}_{beech} \frac{(1-\nu_{bio}) \cdot (1-\phi_{bio})}{(1-\nu_{torbech}) \cdot (1-\phi_{torbech})} \tag{3.20}$$

ν_i are the mass fractions of humidity contented in the biomass at the inlet and outlet of R-TORR, while ϕ_i represent the fractions of ash in the same components (Table A.1). Considering the reactions of the volatile products, the fractional conversion of biomass is evaluated for each component from reaction 3.22 where A and B are parameters from Dossow's model [21] that depend on the volatile product (Table A.9). This is with the exception of water since the mass balance is closed converting the remaining biomass into it. Thus:

$$X_{\mathrm{H_2O}} = 1 - \sum_i X_i \tag{3.21}$$

$$X_i = A \cdot T^B_{torr} \tag{3.22}$$

Furthermore, the HHV of the torrefied product is estimated in the TORCALC through equation 3.23 [21]

$$HHV_{daf} = LHV_{daf} + 212.1265 \cdot H_{daf} + 0.8 \cdot (O_{daf} + N_{daf}) + 24.4 \cdot \frac{H_2O_{ar}}{(1-\nu)(1-\phi_{ash,dry})} \tag{3.23}$$

H, O, N, and H_2O are the values from the proximate analysis of the torrefied products, while $\phi_{ash,dry}$ and ν are the ash and moisture content. LHV_{daf} is obtained from:

$$LHV_{torr,daf} = LHV_{biomass,daf} \cdot (0.001352 \cdot T_{torr} + 0.804977) \tag{3.24}$$

C-PRE To conclude, the C-PRE calculator block computes some important and useful parameters of the pretreatment simulation such as torrefaction mass yield, energy yields, and carbon conversion. The yields are calculated by considering the values of biomass (*bio*) and torrefied biomass (*tor*) in terms of mass flow and HHV.

Both values are expressed on a dry base.

$$\eta_{mass} = \frac{\dot{m}_{tor}}{\dot{m}_{bio}} \tag{3.25}$$

$$\eta_{energy} = \eta_{mass} \frac{HHV_{tor}}{HHV_{bio}} \tag{3.26}$$

Additionally, the C-PRE estimates the carbon conversion η_C of the pretreatment process in $\left[\frac{kg_{C,tor}}{kg_{C,bio}}\right]$.

$$\eta_C = \frac{\dot{m}_{C,tor}}{\dot{m}_{C,bio}} \tag{3.27}$$

It is given by the ratio of carbon content in the mass flows of torrefied biomass $\dot{m}_{C,tor}$ to feedstock biomass $\dot{m}_{C,bio}$. Therefore, the ultimate analysis values ψ (Table A.1) are used to calculate the carbon flow rate, starting from the mass flow rates of MIS, BECH, TORMIS and TORBECH.

$$\dot{m}_{C,bio} = \dot{m}_{mis} \cdot (1 - \nu_{mis}) \cdot (1 - \psi_{mis}) + \dot{m}_{beech} \cdot (1 - \nu_{beech}) \cdot (1 - \psi_{beech}) \tag{3.28}$$

$$\dot{m}_{C,tor} = \dot{m}_{tormis} \cdot (1 - \nu_{tormis}) \cdot (1 - \psi_{tormis}) + \dot{m}_{torbech} \cdot (1 - \nu_{torbech}) \cdot (1 - \psi_{torbech}) \tag{3.29}$$

3.1.3. Gasification

The gasification process is modeled as a three-step process involving three main blocks: R-PYRO, R-NIT and R-GAS. Other blocks, such as compressors and heaters, are used to complete the overall process as is represented in Figure 3.3. In total, the blocks used, and listed in Table A.3 are four Compr blocks, three heaters, one RYield reactor, one RStoic reactor and a RGibbs reactor.

Gassification flowsheet description

After completing the pretreatment, the torrefied and ground biomass is fed in the gasification process through FUEL-IN connected to the R-PYRO block that represents the first step of the gasification. Its aim is to break down the torrefied biomass (TORMIS and TORBECH) in its main constituents that are C, N_2, H_2O, O_2, H_2, CL_2, S and ashes. This is necessary because the downwards reactor R-GAS can only

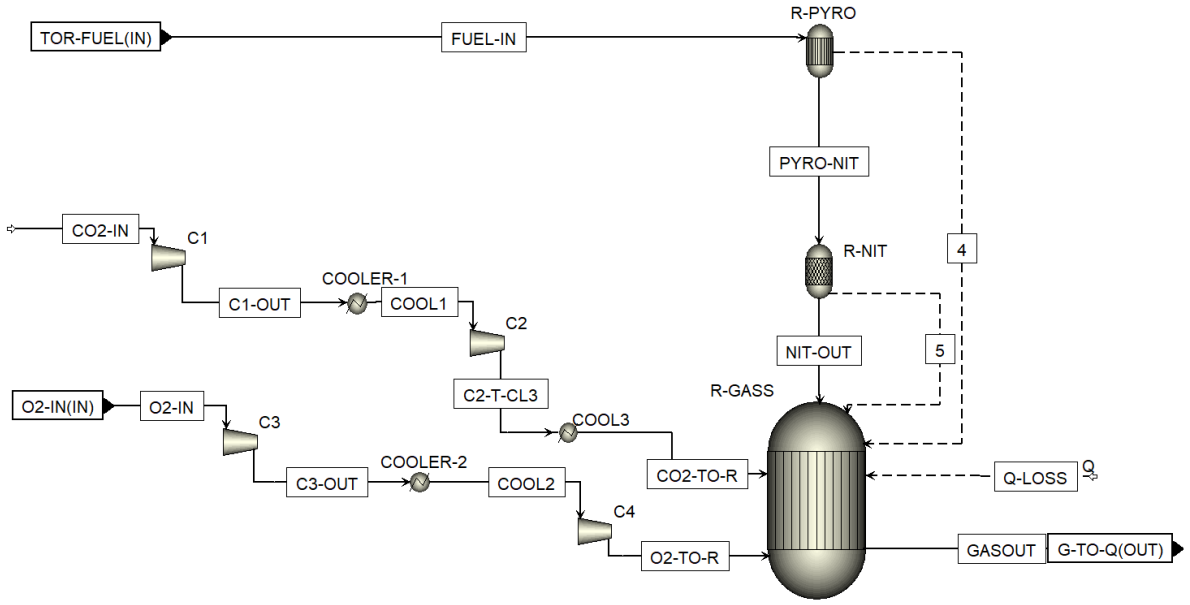

Figure 3.3.: Gasification flowsheet

treat conventional components that take part in the phase and chemical equilibrium. Therefore, TORMIS and TORBECH themselves cannot be introduced in the RGibbs reactor since it is a non-conventional component and, by definition, does not participate in equilibrium calculations.

Among the specified output component of R-PYRO, C is declared as a CIPSD substream while ashes are a non-conventional component (ASH). ASH component is specified to have 100% of ash content in the PROXANAL and ULTANAL attributes in the component attribute sheet of the block. Outlet component yields are extracted from the ultimate and proximal analysis of TORMIS andTORBECH in the C-PYRO calculator block, which changes the previous placeholder values in the block. Thus, a stream of several components mentioned above is sent to the R-GAS reactor where syngas is produced. However, the stream passes through another block before reaching the gasifier for the last step of the gasification. Indeed, PYRO-NIT stream enters the second stage reactor, R-NIT where the generation of nitrogen-based pollutants is separately modeled. The involved reactions are 3.30 and 3.31 which model the

generation of ammonia and hydrogen cyanide.

$$0.5\,N_2 + 1.5\,H_2 \longrightarrow NH_3 \tag{3.30}$$

$$0.5\,N_2 + 0.5\,H_2 + C \longrightarrow HCN \tag{3.31}$$

The fractional conversion of nitrogen is calculated in the dedicated calculator block C-NIT. Once those 2 steps are concluded, the third and final step of gasification occurs. In order to model it, a RGibbs reactor is used. The products generation is based on Gibbs free energy minimization taking into consideration the possible outlet components specified in the block's products. However, not all inlet components participate in the equilibrium. Indeed, NH_3 and HCN are declared completely inert because otherwise, it would lead to an almost total transformation of these nitrogen compounds in N_2. Furthermore, also carbon is declared as inert with a fraction of 0.1 to represent a 99% carbon conversion. Therefore, the declared possible outlet products are all the components that could be output products of the RGibbs reactor. They are: N_2, H_2O, H_2S, COS, C, NH_3, HCN, HCL, H_2, CO_2, S, CH_4.

Additionally, two more material streams are fed to the R-GAS. CO2-IN has a specified volume flow rate of 11.91 m^3/h of CO_2 as a carrier gas for pneumatic transport of the solid fuel. With the optimum carrier gas loading being about 300 kg solid/actual m^3 gas, the required CO_2 mass flow rate is calculated [21]. The CO_2 is assumed to be obtained from the recycle of CO_2 extracted in the AGR section where most of the carbon dioxide is removed from the produced syngas. Differently, O2-IN introduce the gasifying agent (O_2) necessary for the gasification process. Its mass flow rate is fixed to achieve a design specification of 1500 $°C$. CO_2 and O2 are both compressed and cooled in two stages to reach the required pressure of 37 bar. While CO_2 is cooled twice and enters the gasifier at 50 °C, O_2 only encounters a cooler just in the first compression stage and gets in at around 284 °C.

Heat streams from R-PYRO and R-NIT to R-GAS model the auto-thermal process of the different stages of the gasification, whereas Q-LOSS heat stream model the heat losses in the gasification reactor.

Finally, from the gasification process exit a mixture of gas which will be treated in the following section in order to obtain a clean synthetic gas for the Fischer-Tropsch synthesis.

Gasification Calculations

To run the simulation, 3 calculator blocks are required.

C-PYRO Here, the product yields for the R-PYRO block are imported from the ultimate and proximate analysis data of the torrefied biomass and converted in the component yields (equation 3.32). Essentially, the ultimate percentage value (μ_i) is multiplied by the solid percentage of the torrefied biomass since the latter has a humidity content of 10% (ν) and the component attributes are specified on a dry basis. In this way, the torrefied biomass TORMIS and TORBECH are decomposed in its constituents.

$$\lambda_i = \frac{\mu_i}{100}\,(1-\nu) \tag{3.32}$$

Regarding H_2O yield, this is simply imported from the moisture content indicated in the proximate analysis.

C-NIT The purpose of this block is to calculate the fractional conversion of nitrogen for reactions 3.31 and 3.30. The necessary equations are 3.33 and 3.34 where f_N is equal to 0.138 and represents the mass fraction of volatilized nitrogen evolving as HCN [21].

$$X_{NH3} = \frac{1}{5 + \dfrac{17}{27}\,\dfrac{f_N}{1-f_N}} \tag{3.33}$$

$$X_{HCN} = \frac{17}{27}\,\frac{f_N}{1-f_N}\,X_{\mathrm{NH_3}} \tag{3.34}$$

C-QLOSS Similarly to the pretreatment section, the heat losses of the gasification reactor are modeled as a fraction of the Lower Heating Value (LHV) times the torrefied biomass mass flow rate. Therefore:

$$\dot{Q}_{L,gasifier} = -0.03 \cdot \dot{m}_{torbio} \cdot HHV_{torbio} \tag{3.35}$$

C-GAS As well as for the pretreatment, some important parameters useful for the model analysis are calculated. The C-GAS block calculates the efficiency of the

process, the CGE and H_2 recovery. The CGE is calculated with equation 3.36,

$$CGE = \frac{HHV_{syn} \cdot \dot{m}_{syn}}{\dot{m}_{fuel} \cdot HHV_{tor}} \tag{3.36}$$

where HHV_{syn} and HHV_{tor} are the higher heating values of the produced syngas and the torrefied biomass fed to the gasifier, while $\dot{m}_{syn}$ and $\dot{m}_{tor}$ are the mass flow rates. HHV_{syn} is calculated with equation 3.37 and HHV_{tor} is calculated in the TORCALC block on a dry and ash-free basis. Therefore, an appropriate conversion to an as-received basis is necessary since the torrefied biomass contains amounts of ash and moisture contents as specified in Table A.7.

$$HHV_{syn} = HHV_{\mathrm{H_2}} \cdot y_{\mathrm{H_2}} + HHV_{\mathrm{CO}} \cdot y_{\mathrm{CO}} + HHV_{\mathrm{NH_3}} \cdot y_{\mathrm{NH_3}} + HHV_{\mathrm{ch_4}} \cdot y_{\mathrm{CH_4}} \tag{3.37}$$

For the calculation of HHV_{syn} the higher heating values of each component are multiplied by the corresponding mass fraction in the syngas. To obtain the overall efficiency of the gasification process, the compressor contribution is added to the CGE formula:

$$\eta_{gasification} = \frac{HHV_{syn} \cdot \dot{m}_{syn}}{\dot{m}_{fuel} \cdot HHV_{tor} + W_{comp}} \tag{3.38}$$

where W_{comp} is the sum of each compressor involved (C1, C2, C3, C4).

Additionally, H_2 recovery is calculated as the ratio between the hydrogen amount in the torrefied biomass to the amount in the syngas.

3.1.4. Quenching

The syngas that is produced in the gasification hierarchy is a raw gas with a high level of impurities and ashes. For this reason, the gas needs to be treated to be efficiently exploited in the FT synthesis. Quenching is the first step in this process. The quenching subsystem focuses on the cooling of the raw gas and its cleaning from impurities. The model employs the blocks described in Table A.4 and it involves two main steps where the gas is treated, represented by the quenching and scrubber tank (R-QUANCH and SCRUBBER) in Figure 3.4.

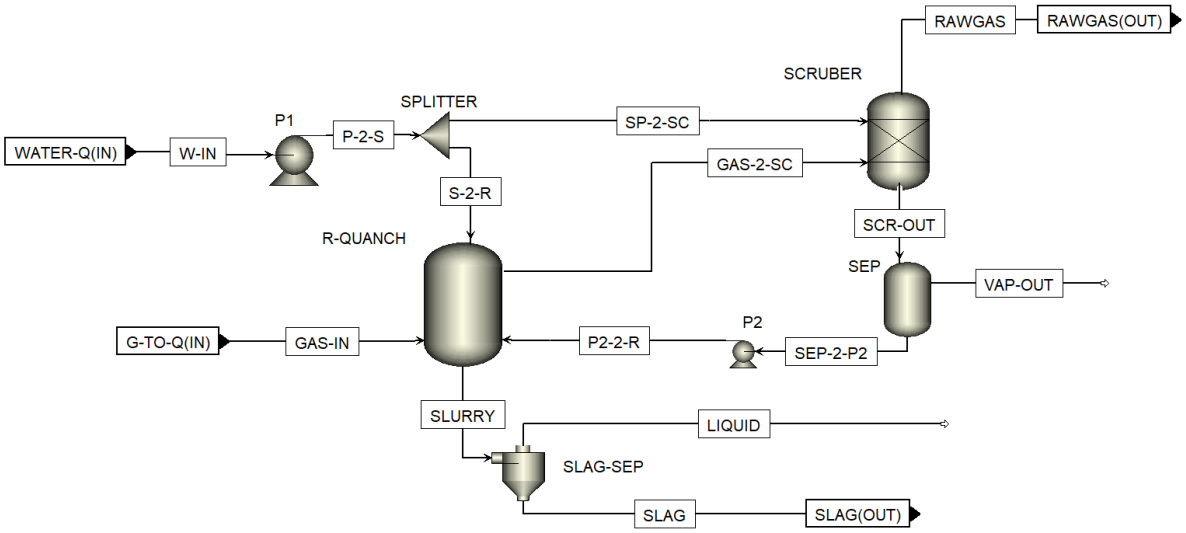

Figure 3.4.: Gas quench flowsheet

Quench hierarchy setup

For the quench subsystem, a different property method with respect to PR-BM method is selected. This comes from the need to model different solubility for different components. As a matter of fact, NH_3 and HCN subjected to quenching and water scrubbing, have good solubility in water. However, other components such as CO_2 and H_2S, which are products of the gasification, have a low solubility in water and they can be removed only with specific solvents. Therefore, a different property method is necessary to avoid the gas to be cleaned also form CO_2 and H_2S in the quench section, which would represent a less rigorous modeling of the process. The selected property method is ENRTL-RK and the free-water method is changed to STEAM-TA.

Additionally, as already mentioned in Paragraph 3.1.1, for the quench simulation it is necessary to specify a set of sour reactions and to declare some components as Henry's components to allow an apparent simulation approach.

Quench flowsheet description

The row gas from the gasification hierarchy is fed into the R-QUENCH tank where it is cooled down by water. Owing to the water, impurities such as HCl are dissolved

and partially separated from the gas. At the same time, ashes and ionic components generated from the sour reactions are totally dissolved in water and exit as slurry towards the SLAG-SEP block. Here, this latter separates the slag, mainly composed of ashes, and the liquid phase containing wastewater used in the process, ionic species, gas impurities such as HCl, COS and solid carbon.

The water feeds the system by means of W-IN and it is immediately compressed by P1 at the pressure of the quench tank. The block SPLITTER then distributes the water between the quench reactor and the wet scrubber. In the wet scrubber (SCRUBBER), the water absorbs some remaining impurities of HCl, solid particles of carbon or ashes in the gas. It is modeled with a Sep block that indicates the split fraction of each component of the inlet streams to a specific outlet stream. They are listed in table A.10, except for water whose split fraction is calculated in the C-SCRUB block. Therefore, after the quench, the gas freed from most of its original impurities directly enters the scrubber through GAS-2-SC where it is further cleaned. Subsequently, a cleaner level of gas exits from the scrubber and is directed to the following gas treatment section: acid gas removal. The water employed in the scrubber is then recirculated in the quench tank. To do so it is necessary to bring the water pressure level back to 36 bar with the pump P2.

Quench Calculations

In the quench section, only two blocks are implemented. C-QUENCH estimates the specific amount of water required per kg of outlet gas in the quenching process. It is calculated as the ratio of the water flow rate to the outlet gas flow rate:

$$\tau = \frac{\dot{m}_{\mathrm{H_2O}}}{\dot{m}_{\mathrm{gas}}} \tag{3.39}$$

C-SCRUB calculates the fraction of water exiting by SCR-OUT in the SCRUBBER block. The calculation is made assuming a H_2O/CO ratio of 1.3. From this value, the mass flow rate of water that needs to exit in the RAWGAS stream ($\dot{m}_{\mathrm{H_2O},rg}$) is obtained by multiplying the mass flow of CO. Therefore, the split fraction (λ) of water to SCR-OUT is calculated as in equation 3.40, where $\dot{m}_{\mathrm{H_2O},in}$ is the total water flow rate

entering in the scrubber.

$$\lambda = 1 - \frac{\dot{m}_{H_2O,rg}}{\dot{m}_{H_2O,in}} \tag{3.40}$$

3.1.5. Water-Gas Shift

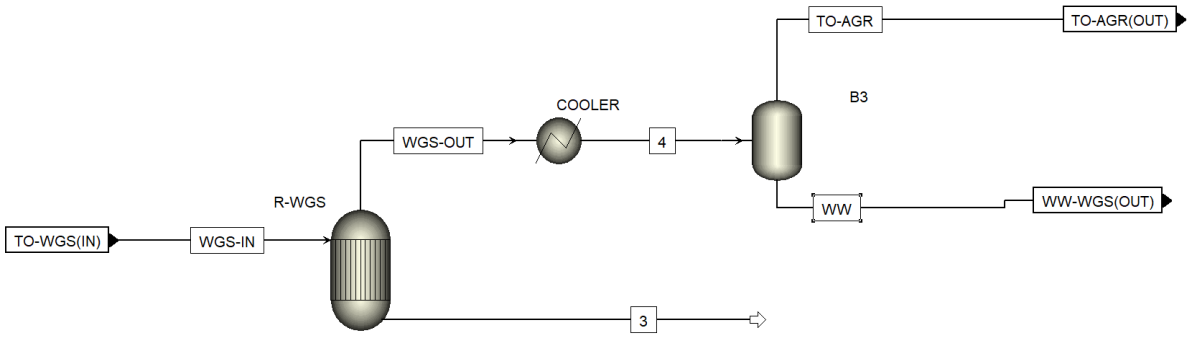

Figure 3.5.: Water-Gas shift flowsheet

In the WGS hierarchy block the water gas shift reaction is applied to adjust the H_2/CO molar ratio to 2.1. The flowsheet is very simple as only three blocks are used. They are a REquil reactor, a Heater and a Flash2 block.

However, before entering the WGS hierarchy block, the gas from the quench section encounters a Changer block that changes the stream class from MCINCPSD to CONV. Thus, as already explained in Section 3.1.1, every hierarchy subsequent to this block works with conventional streams.

WGS flowsheet description

The raw gas coming from the quench section firstly feds the R-WGS where the water-gas shift reaction occurs. A calculator block is used to calculate the reaction extent in order to obtain a H_2/CO molar ratio of 2.1 in the syngas. Once it exits the reactor, it is cooled down at 30°C and then it is separated from the liquid phase. As a result, a liquid stream composed mainly of water, and a gaseous stream of syngas directed towards the acid gas removal exit separately from the B3 block.

WGS calculation

Two calculator blocks are employed in this section. C-REXTEN is used to calculate the molar extent of the reaction for the WGS in block R-WGS while C-WGS estimate the H_2/CO ratio to simply assess the correctness of the calculation in C-REXTEN.

C-REXTEN The molar extent of the reaction is calculated considering the equation 3.41 with n_i and n_i' being the molar quantity of element i before and after the reaction, respectively. ν_i is the corresponding stoichiometric number.

$$\xi = \frac{n_i' - n_i}{\nu_i} \tag{3.41}$$

Since only the molar quantity of H_2 and CO in the gas at the beginning of the reaction is known, the extent of the reaction cannot be directly estimated with 3.41. However, the reaction extent can be found first considering that $\xi = \xi_{H_2} = \xi_{CO}$. Therefore:

$$\frac{n'_{H_2} - n_{H_2}}{\nu_{H_2}} = \frac{n'_{CO} - n_{CO}}{\nu_{CO}} \tag{3.42}$$

At this point, $n'_{CO} = \frac{n'_{H_2}}{2.1}$ is substituted in 3.42, since the target H_2/CO ratio is 2.1. ν_{CO} ν_{H_2} are respectively 1 and -1 considering the WGS stoichiometry, hence what is obtained is:

$$n'_{H_2} - n_{H_2} = n_{CO} - \frac{n'_{H_2}}{2.1} \tag{3.43}$$

Finally, solving the equation for n'_{H_2} it is possible to calculate the extent of reaction with equation 3.41.

3.1.6. Acid Gas Removal

The AGR is a further step in the gas treatment before its synthesis and it consists of the removal of H_2S and CO_2. In order to do so, a specific solvent (DEPG5 in Table A.1) is used to dissolve and absorb the acid gasses in the syngas. To model the solubility of the different components of the syngas, the values in Tables A.11 are specified in the property environment in the `Model\Binary interaction\HENRY-1` folder accordingly with Dossow's model [21]. The block specifications are described in Table A.5

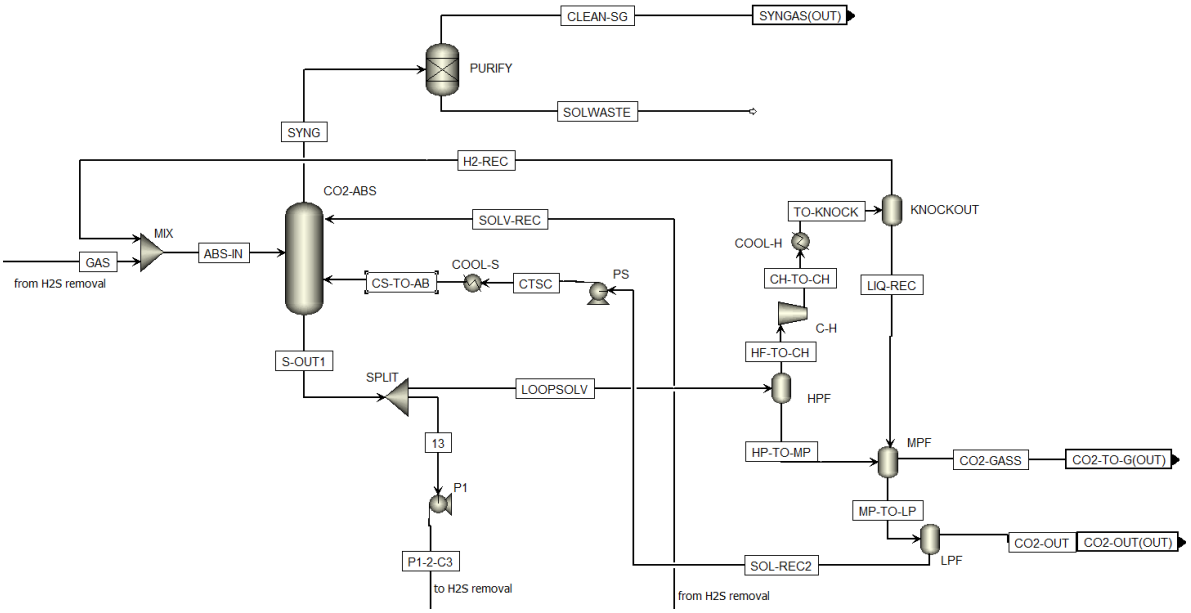

Figure 3.6.: Acid Gas Removal Flowsheet - CO_2 subsection

AGR flowsheet description

H_2S removal occurs in the first part of the process. The syngas from the WGS hierarchy block firstly is compressed and heated before entering the ABS-H2S block. Here, the syngas contacts the solvents coming from the CO_2 removal and gets into the H_2S absorber by the SOL-ABS stream. The reaction is modeled by defining the fraction of each component that is split into the outlet GAS stream (Table A.12). This stream contains the cleaned gas from H_2S that heads towards the CO_2 removal part of the process.

The solvent rich in H_2S, gets through the CONC-H2S block after being re-pressurized and heated. This block works as a concentrator for H_2S in the solvent desorbing and recirculating CO and H_2. It uses nitrogen as stripping gas which is compressed and heated from ambient conditions. The nitrogen mass flow rate is settled to be the 2.25% of the S-OUT2 stream. As for the ABS-H2S, the split fractions for the REC stream are specified in accordance with Table A.13. In this way, the components absorbed by the solvent that are not H_2S are re-circulated inside the H_2S absorber.

The same solvent is used for the CO_2 removal. However, before being employed in the process, the solvent needs to be recovered and separated from H_2S in a stripper

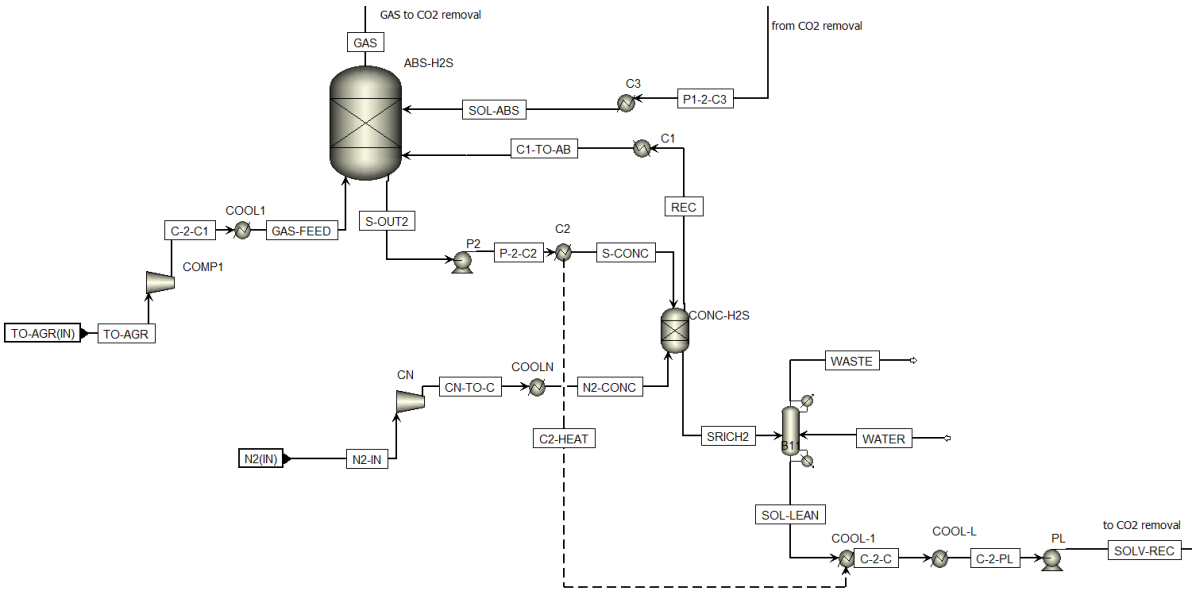

Figure 3.7.: Acid Gas Removal Flowsheet - H_2S subsection

column STRIP. Thanks to a water flow rate fixed as 1% of the solvent stream, most of H_2S is separated exiting from the WASTE stream while the cleaned solvent is cooled down by means of COOL-1 and COOL-L. Finally, the solvent is re-pressurized and sent to the CO_2 absorber, only after being cooled down by COOL-1 and COOL-L. Its heat is partially sent to C2 throughout the C2-HEAT stream.

The solvent is fed to the CO_2 absorber, as well as the treated gas free from H_2S after being mixed with recovered hydrogen dissolved in the solvent. The syngas, with a lower CO_2 content exit the CO2-ABS block through the SYNG stream. It is further purified by separating some remaining trace of DEPG5 and H_2S in the gas to have a desired amount of 9 ppb. The CO2-ABS specifications are shown in Table A.14.

The absorbed CO_2 originally in the gas comes out from the S-OUT1 stream dissolved in DPG5. Employing the SPLIT block, one part of the solvent is pressurized and sent back to the H_2S absorber while the other part is subjected to a three-step flash separation process to separate the CO_2 from the solvent. The high-pressure step represented by the HPF block aims to recover quantities of CO and H_2 absorbed by the solvent. They are re-circulated and re-injected into the syngas by the H2-REC which are then mixed using the MIX block. Before this, the recovered gases are compressed and cooled so they can potentially be separated from liquid traces. The

intermediate pressure step (block MPF) is regulated by a design spec in order to have a CO_2 flow rate equal to the CO2-IN stream in the gasification section (3.1.3). The reason behind this is that part of the CO_2 contained in the syngas is assumed to be recirculated as a carrier gas for the gasification. The last, low-pressure step at 1.5 bar completely separates the remaining CO2 and recovers the solvent that is employed again in the CO2-ABS block by the SOL-REC2 stream after being pressurized and cooled down.

In the end, the clean syngas is carried to the Fischer-Tropsch synthesis exiting the AGR section by CLEAN-SG.

AGR calculations

Two calculator blocks are employed in the AGR section. One calculates the water requirement for the striping column and the other calculates the percentage removal of CO_2 and H_2S.

C-WATER It calculates the mass flow rate of water fed to the column stripper B11 assuming it to be 1% of SRICH2 mass flow rate.

C-AGR As already mentioned, this block calculates two useful parameters as CO_2 and H_2S percentage removal. They are calculated considering the mass flow at the inlet and outlet of the hierarchy block of each substance in the syngas. Therefore, the percentage removal is calculated in accordance with equation 3.44.

$$\%REM_i = \frac{\dot{m}_{i,in} - \dot{m}_{i,out}}{\dot{m}_{i,in}} \tag{3.44}$$

3.1.7. Fischer-Tropsch Synthesis and Upgrading

Once the syngas is treated and cleaned from all impurities, it can be employed in the Fischer-Tropsch synthesis to produce the final products. The dedicated hierarchy block is simple, involving only three blocks that are described in Table A.6.

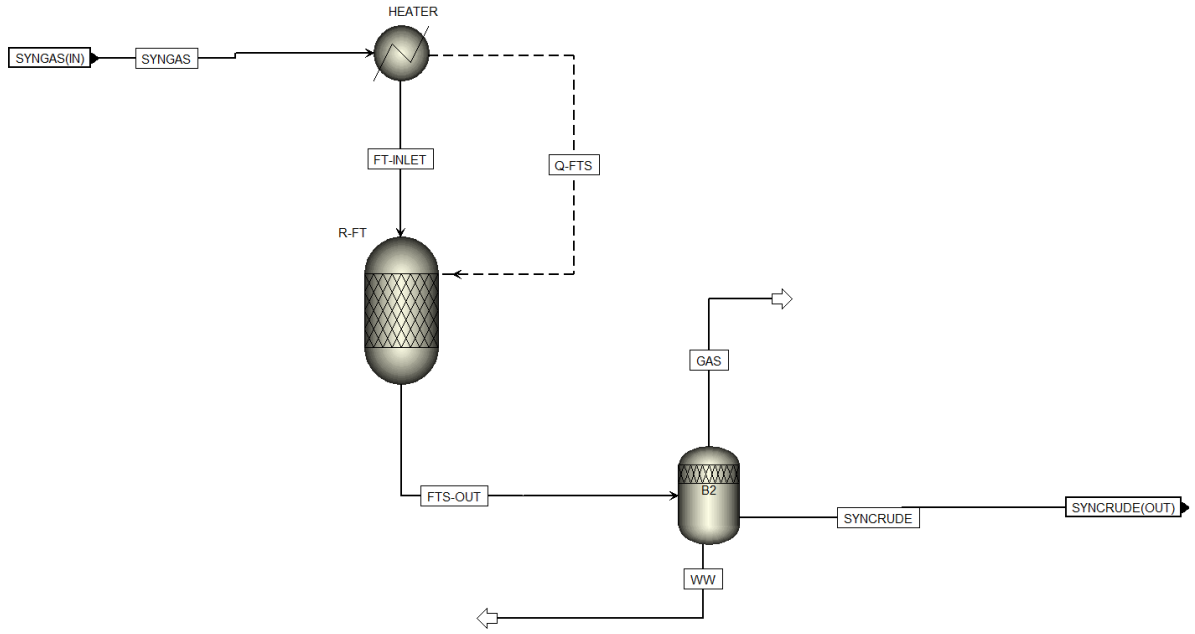

Figure 3.8.: Fischer-Tropsch Synthesis flowsheet

Flowsheet description

The cleaned syngas coming from the treatment processes is first heated and then fed to the R-FT block. The thermal requirement is provided by Q-FTS stream. Here, the synthesis occurs, accordingly with the reactions in Table A.8 that models the process. The fractional conversion of CO is calculated considering the kinetic model adopted by Dossow in his work [21] and the obtained results. Reactions are divided into three categories depending on their products: olefins (r_1), paraffins (r_2) and methanation reaction ($_3$) that generate CH_4. The CO fractional conversion of each reaction category can be calculated starting by considering the equations of the rate of reaction.

$$r_{CO} = -r_1 \cdot \left(1.08 + 9.165(1-\alpha)^2 \cdot \exp\left(-272.96\left(\frac{1}{T} - \frac{1}{483}\right)\right)\right) \tag{3.45}$$

$$r_2 = 0.08 \cdot r_1 \tag{3.46}$$

$$r_3 = 9.165 \cdot r_1 \cdot (1-\alpha)^2 \cdot \exp\left(-272.96\left(\frac{1}{T} - \frac{1}{483}\right)\right) \tag{3.47}$$

The rate of reaction is directly proportional to the produced product and the reacted reagents. Therefore, the reacted CO is also proportional to the rate of reaction, which

can be expressed in terms of the fraction of CO converted (χ_{CO}). For this reason, it is possible to state that:

$$\frac{\chi_{CO}}{\chi_1} = \frac{r_{CO}}{r_1} = \left(1.08 + 9.165(1-\alpha)^2 \cdot \exp\left(-272.96\left(\frac{1}{T} - \frac{1}{483}\right)\right)\right) \tag{3.48}$$

The minus sign is neglected as it represents the reaction direction and it is not of interest for the purpose of this analysis.

At this point, since α and χ_{CO} values are known from Dossow's work [21], χ_1 can be calculated. χ_2 is calculated considering equations 3.46, 3.47 and the same relationship of proportionality mentioned above, can be expressed as:

$$\chi_2 = \frac{r_2}{r_1}\,\chi_1 \tag{3.49}$$

On the other hand, χ_3 is obtained considering that: $\chi_{CO} = \chi_1 + \chi_2 + \chi_3$

Finally, with $\chi_{CO} = 0.55$, $\alpha = 0.92$, and $T = 220$ being the CO conversion, the chain growth probability and the FTS temperature respectively, the obtained results are: $\chi_1 = 0.496$, $\chi_2 = 0.03752$, $\chi_3 = 0.0.04348$. Dividing this result by the number of reactions of each category ($n_1 = n_2 = 31$,$n_3 = 1$), the fractional conversions of CO for each reaction in Table A.8 are specified in the R-FT block.

What exits from the FTS reactor is a mixture of organic products, water and gases that are separated in the subsequent block. The organic component of the mixture, made of hydrocarbons of a wide range of lengths, is sent to the upgrading hierarchy block. Here, the FTS product is split in fractions into different end products with a Sep block (Figure 3.9), with the consideration of the chain length of the components. The SNG stream contains synthetic natural gas, only methane in this case. NAPHTHA contains hydrocarbons from C_2 to C_7 while the JET-FUEL streams includes C_8 up to C_{16}. GAS-OIL and WAXES have C_{17} to C_{22} and C_{23+}, respectively. The UPGRADE block is specified so that every stream contains the mentioned components, except for SYNG that include the remaining gases that form syngas closing the mass balance.

3.2. Modified case simulation models

The base case simulation model (Section 3.1) is optimized replacing the conventional autothermal gasification with allothermal plasma gasification in the first case and

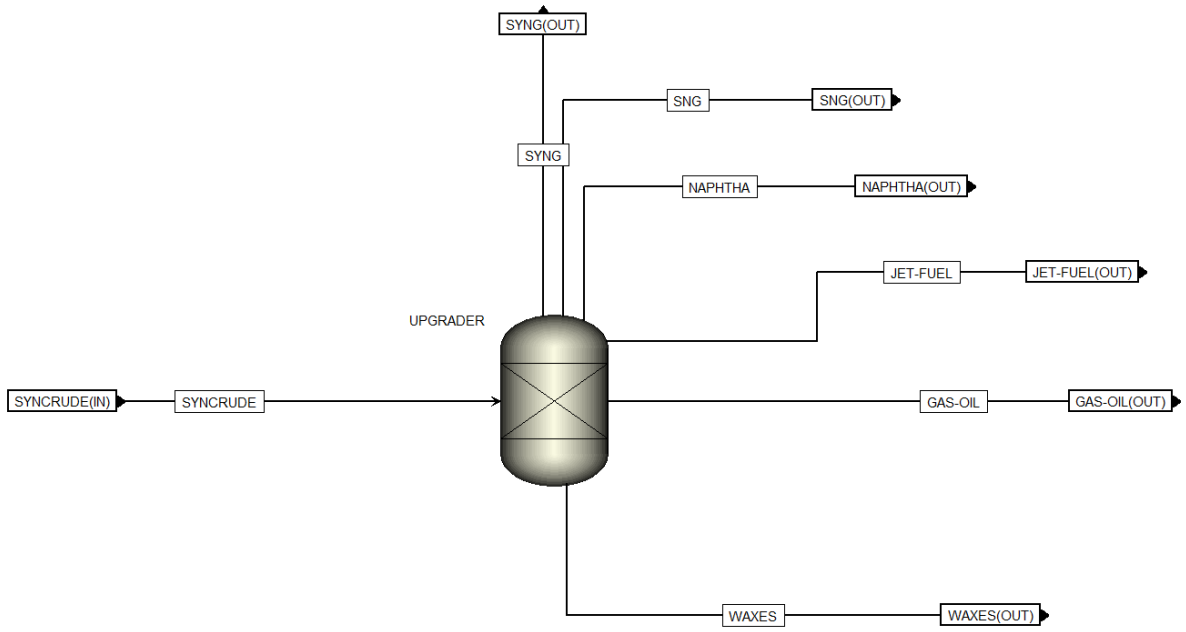

Figure 3.9.: Upgrading Flowsheet

conventional torrefaction with GP torrefaction. The two modifications are described in Subsection 3.2.1 and 3.2.2.

3.2.1. Modification 1: plasma gasification

To model the plasma gasification process, some changes are brought to the gasification hierarchy subsystem. As can be noticed by comparing the gasification flowsheet (Figure 3.3) of the base case model with the gasification flowsheet of the optimized model (Figure 3.10), the heat streams *5* and *6* are removed. In this way, the process is no longer modeled as autothermal, but rather as allothermal. An external heat source therefore is needed. The heat is supplied by a plasma torch modeled by a steam stream which is heated up to 4000 °C before entering the gasifier, by a heater that represents the AC arch for the ionization. Inevitably the temperature of the exiting syngas increases with respect to the conventional gasification temperatures. For this reason, the outlet temperature is set to 2000 °C by a design specification controlling the oxygen flow input.

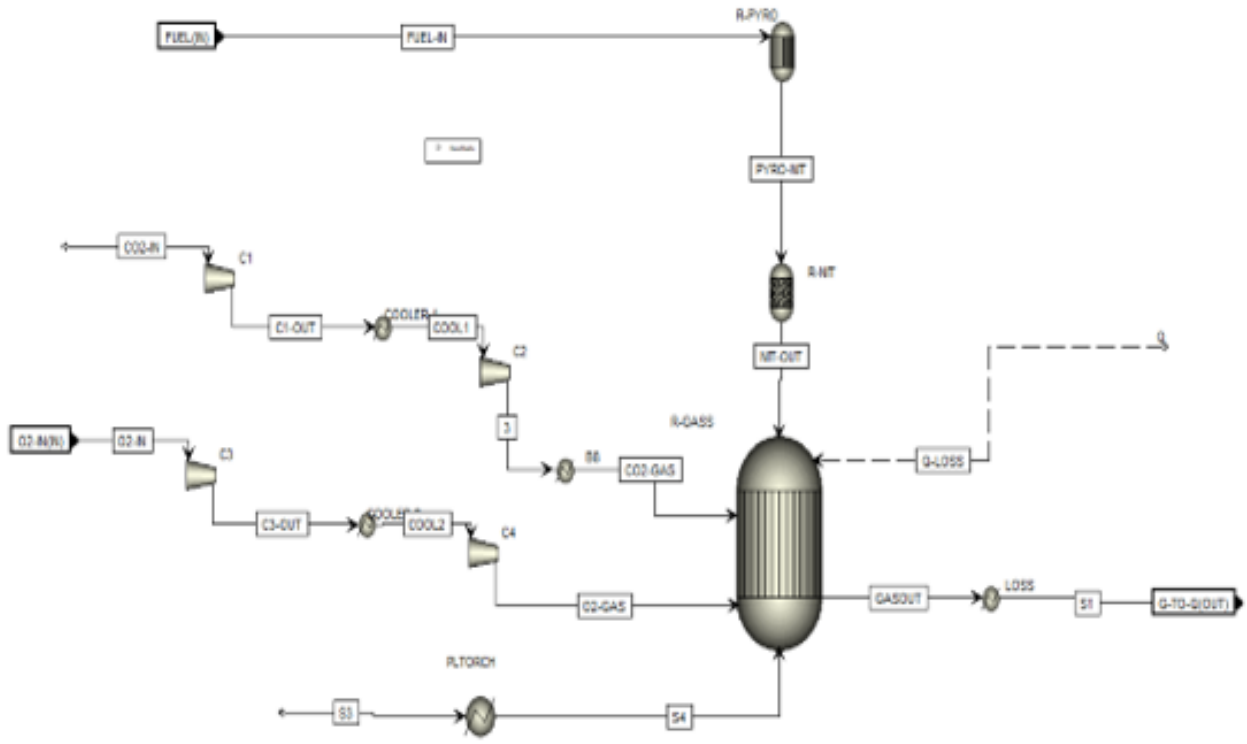

Figure 3.10.: Plasma gasification flowsheett

Table 3.2.: Torrefaction block reaction with GP torrefaction yields

$MIS \longrightarrow TORMIS$	$X_{tormis} = 0.45$
$MIS \longrightarrow \gamma_{H2O}\,H_2O$	$X_{H_2O} = 0.4$
$MIS \longrightarrow \gamma_{CO}\,CO$	$X_{CO} = 0.05$
$MIS \longrightarrow \gamma_{CO2}\,CO_2$	$X_{CO_2} = 0.1$
$BEECH \longrightarrow TORBECH$	$X_{torbech} = 0.45$
$BEECH \longrightarrow \gamma_{H2O}\,H_2O$	$X_{H_2O} = 0.4$
$BEECH \longrightarrow \gamma_{CO}\,CO$	$X_{CO} = 0.05$
$BEECH \longrightarrow \gamma_{CO2}\,CO_2$	$X_{CO_2} = 0.1$

3.2.2. Modification 2: gas-pressurized torrefaction

For the modeling of the gas-pressurized torrefaction, it is necessary to give different specifications to streams and blocks on the basis of data obtained by related experiments. Data from Tong et al [65] are used, in particular proximate and ultimate

analysis values and yields of the torrefing process. Proximate and ultimate analysis values are specified in the feedstock input stream *FEED-WET*. Moisture contents are kept as in the base case and other contents are specified on a dry basis (db). This is done also for the torrefied product whose fuel analysis is specified in the *R-TORR* block in the component attribute section. Fuel analysis is shown in Table A.15.

The effect of gas-pressurized torrefaction is given by the product yields of the torrefaction. Approximated values are integrated in the *R-TORR* block specified as fractional conversions of the respective reaction. In Table 3.2 the reactions with the respective product yields are represented.

4. Results

In this chapter, the results obtained from the Aspen model for the base case simulation and the modified cases are described and discussed. The results highlight the performances of the processes in terms of energy yields and carbon conversions, showing the evolution of the energy and carbon content throughout the process.

4.1. Method

The energy and carbon yields are calculated in the three cases for each main section of the process: pre-treatment, gasification, gas conditioning and synthesis.

The energy yield is calculated considering the energy contained in the inlet and outlet streams of each section, following equation 4.1, where $\dot{m}$ is the mass flow rate of the inlet and outlet streams, and HHV is the respective higher heating value.

$$\eta = \frac{\dot{m}_{outlet} \cdot HHV_{outlet}}{\dot{m}_{inlet} \cdot HHV_{inlet}} \tag{4.1}$$

In particular, referring this equation to each section, the formulas are:

$$\text{Pre-treatment} : \eta_{pre-treatment} = \frac{\dot{m}_{feedstock} \cdot HHV_{feedstock}}{\dot{m}_{torrefied\ product} \cdot HHV_{torrefied\ product}} \tag{4.2}$$

$$\text{Gasification} : \eta_{gasification} = \frac{\dot{m}_{torrefied\ product} \cdot HHV_{torrefiedproduct}}{\dot{m}_{raw\ syngas} \cdot HHV_{raw\ syngas}} \tag{4.3}$$

$$\text{Conditioning} : \eta_{conditioning} = \frac{\dot{m}_{raw\ syngas} \cdot HHV_{raw\ syngas}}{\dot{m}_{clean\ syngas} \cdot HHV_{clean\ syngas}} \tag{4.4}$$

$$\text{Synthesis} : \eta_{synthesis} = \frac{\dot{m}_{clean\ syngas} \cdot HHV_{clean\ syngas}}{\dot{m}_{liquid\ product} \cdot HHV_{liquid\ product}} \tag{4.5}$$

$$\tag{4.6}$$

Torrefied product refers to the torrefied biomass exiting from the pre-treatment and entering the gasification. Raw syngas refers to the syngas produced by the gasification headed to the conditioning section from where it exits as clean syngas. The liquid product is the mixture of paraffin and olefin generated by the synthesis reactions in table A.8. The overall energy yield of the whole process is obtained by multiplying each yield:

$$\eta_{total} = \eta_{pre\ tratment}\ \eta_{gasification}\ \eta_{conditioning}\ \eta_{synthesis} \tag{4.7}$$

A similar approach is used in order to calculate the carbon yields for the same sections. More specifically, it is the ratio of the carbon contained in the outlet stream of the sub-system to the one in the inlet stream. Therefore, for each section:

$$\text{Pre-treatment} : \gamma_{pre-treatment} = \frac{\dot{c}_{feedstock} \cdot HHV_{feedstock}}{\dot{c}_{torrefied\ product} \cdot HHV_{torrefied\ product}} \tag{4.8}$$

$$\text{Gasification} : \gamma_{gasification} = \frac{\dot{c}_{torrefied\ product} \cdot HHV_{torrefiedproduct}}{\dot{c}_{raw\ syngas} \cdot HHV_{raw\ syngas}} \tag{4.9}$$

$$\text{Conditioning} : \gamma_{conditioning} = \frac{\dot{c}_{raw\ syngas} \cdot HHV_{raw\ syngas}}{\dot{c}_{clean\ syngas} \cdot HHV_{clean\ syngas}} \tag{4.10}$$

$$\text{Synthesis} : \gamma_{synthesis} = \frac{\dot{c}_{clean\ syngas} \cdot HHV_{clean\ syngas}}{\dot{c}_{liquid\ product} \cdot HHV_{liquid\ product}} \tag{4.11}$$

$$\tag{4.12}$$

As well as for the energy yield, the overall carbon yield is given by the product of all contributions. The carbon content for a non-conventional component of a stream such as for the biomass and torrefied biomass is calculated with equation 4.13 and with equation 4.14 for components in mixed substreams as syngas.

$$\dot{c}_i = \dot{m}_i \cdot \mu_i \tag{4.13}$$

$$\dot{c}_{C_xH_yO_z} = x\dot{n}_i \cdot 12 \tag{4.14}$$

$\dot{m}_i$ is the mass flow of the non-conventional component and μ_i the percentage carbon content from the ultimate analysis, while $\dot{n}_i$ is the mole flow rate of a carbon-containing gas in the syngas mixture multiplied by carbon molar weight.

4.2. Presentation and Discussion

The obtained data are gathered in Figure 4.1 for energy yields and efficiency and Figure 4.2 for carbon yields. The data are represented with column graphs showing the energy and carbon yields in each section of the process with the energy and carbon trend stored in the biomass throughout the whole process. Each figure includes three graphs for the base case, plasma gasification modified case and GP torrefaction modified case.

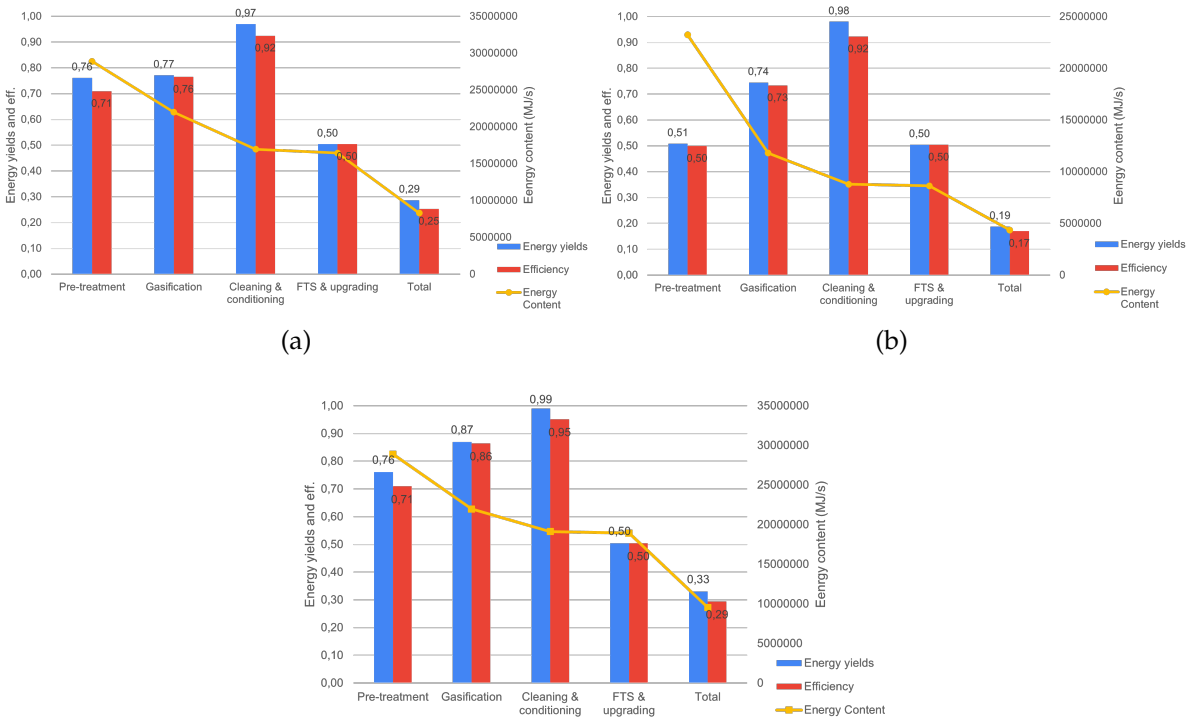

Figure 4.1.: Energy yields, efficiency and energy content evolution in the base case simulation (a), GP torrefaction modified simulation (b) and plasma gasification modified simulation (c)

It can be immediately noticed as the modifications do not affect significantly the energy yield of the conditioning and FTS section. Energy yields in the pre-treatment and gasification section are the ones that vary the most instead, affecting the total energy yield of the whole process. In particular, the same energy yield values of 0.76

can be observed for the pre-treatment section in the base case and plasma gasification modified case, whereas is the GP torrefaction modified case energy yield has a significantly lower value of 0.51. Also, the gasification is affected, but to a lesser extent, with a CGE value of 0.74. For these reasons, the GP torrefaction modified model showcases the worst result with an energy yield of 0.19 compared to 0.29 and 0.33 in the base case and plasma gasification modified case.

Due to the pressure effect, the biomass decomposed at higher grades and more energy is lost in the torrefaction gases. In other words, less energy is stored in the torrefied biomass with respect to AP torrefaction. This is also shown in Figures 4.2a and 4.2b where carbon conversion of the pre-treatment section changes from 0.75 to 0.46 and as a consequence, the carbon content stored in the torrefied biomass as well. On the other hand, a reduction of the carbon content in the biomass corresponds to a higher yield of torrefied gases such as CO_2 and CO and therefore more energy in the gaseous phase of torrefaction products. Since these gases are used as an auxiliary fuel, together with CH_4, to provide heat for the torrefaction process and the biomass drying, the required amount of CH_4 is reduced from 25 $g_{CH_4}/kg_{feedstock}$ in the GP torrefaction case to 5 $g_{CH_4}/kg_{feedstock}$ in the base case with an 80,6% reduction. This can improve the sustainability of the process and reduce the operational cost of the plant. The oxygen required for the gasification is also slightly lower with 0,277 $kg_{O_2}/kg_{feedstock}$ compared to 0,294 $kg_{O_2}/kg_{feedstock}$ in the base case (Table 4.1).

Moreover, the main advantage of the GP torrefaction, is the high concentration of energy in a smaller amount of mass, increasing the energy density. In the base case model, the biomass heating value is subjected to an 18% increase through the torrefaction, compared to a 40.5% increase of the GP torrefaction modified case model. For these reasons mentioned above, GP torrefaction is more suitable for a de-centralized plant rather than an integrated process, where torrefied biomass is directly fed to a gasification unit as in the case of this work. In the former case, torrefied biomass would be stored and transported to other locations for treatment, resulting in reduced transportation emissions and costs, thanks to the higher energy density of the torrefied product.

Figure 4.1c regards the results of the plasma gasification modified model. Plasma gasification has great effects on the energy conversion of the overall process since its

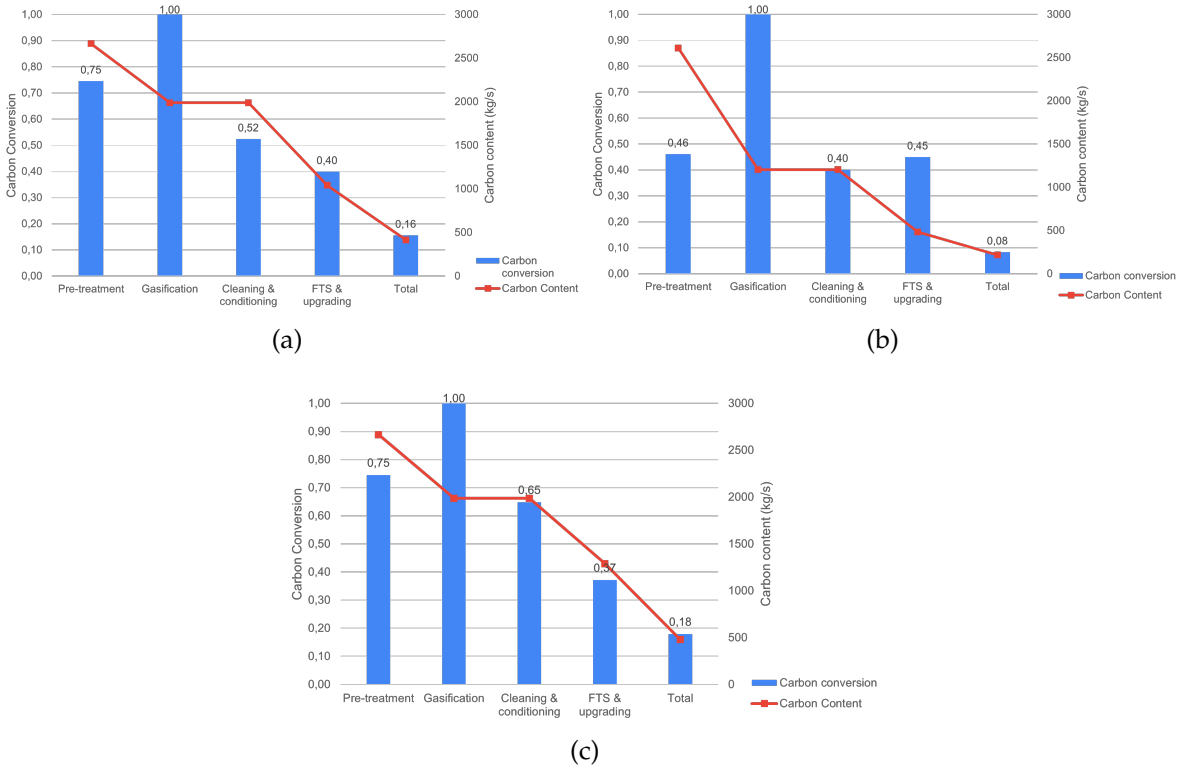

(a) (b) (c)

Figure 4.2.: Carbon yields and content evolution in the base case simulation (a), GP torrefaction modified simulation (b) and plasma gasification modified simulation (c)

energy yield (i.e. CGE) reaches a 0.87 value. Other sections remain overall unchanged while the total process energy yield reaches 0.33. This can be explained by the high temperature provided by the plasma torch, promoting the production of H_2, which dramatically contributes to increasing the heating value of the syngas. Focusing on Figure 4.2c, plasma gasification also has a good impact on the subsequent cleaning and conditioning section raising the carbon conversion. The reason is present in Table 4.1 as H_2/CO ratio of syngas produced in the gasification is 0.041 kg_{H_2}/kg_{CO}, slightly higher respect to the other simulation models. As a consequence, in the conditioning section WGS reactions occur to a lower extent, leading to a lower generation of CO_2 and therefore fewer carbon wastes. This positive effect also contributes to the overall conversion, with 0.18 being the highest among the other two cases, with 0.16 and 0.08 in the base case and GP case respectively.

In Table 4.1 some important parameters and indicators are shown. As already mentioned, in GP torrefaction the natural gas requirement as an energy carrier for the pre-treatment is highly decreased to 0.005 $kg_{CH4}/kg_{feedstock}$ due to enhanced production of torrefied gases used as further energy sources for the process mixed with natural gas. Indeed, torrefaction gases mass flow per the feedstock mass flow is substantially higher than in the other two cases. This is promoted by the pressure involved in the torrefaction that increases the biomass decomposition. If torrefaction gases yield increase and biomass decomposition is enhanced, torrefied biomass yield is reduced to 0.360 $kg_{tor\ bio}/kg_{feedstock}$ with respect to AP torrefaction with 0.646 $kg_{CH4}/kg_{feedstock}$, as reported in Table 4.1.

Table 4.1.: Calculated parameters and KPI

	Plasma gasific.	**GP tor.**	**AP tor.**
Syngas H_2/CO kg/kg	0,041	0,031	0,037
NG requirement $kg_{CH4}/kg_{feedstock}$	0,025	0,005	0,025
O2 requirement $kg_{O2}/kg_{feedstock}$	0,218	0,277	0,294
Torrefaction gases output $kg_{tor\ gas}/kg_{feedstock}$	0,132	0,440	0,132
Torrefied Biomass output $kg_{tor\ bio}/kg_{feedstock}$	0,646	0,360	0,646
Gasific. Syngas output $kg_{syngas}/kg_{feedstock}$	0,865	0,606	0,932
FTS liquid product output $kg_{tor\ bio}/kg_{feedstock}$	0,087	0,039	0,075

5. Conclusions

In this work, alternative solutions to the conventional AP torrefaction and autothermal gasification are investigated. Firstly, a base case simulation model was developed to study and compare the impacts of GP torrefaction and plasma gasification on the original process. In analysing the results obtained in the Aspen Plus simulation models it is possible to draw the following conclusions:

- The modification brought to the base case model, changing the AP torrefaction with GP torrefaction and traditional gasification with plasma gasification do not affect significantly the outcomes of the conditioning and FTS sections. They rather have a substantial impact on the pre-treatment and treatment sections of the processes.
- Plasma gasification has been demonstrated to be a promising technology, showcasing a good increase in performances not only of the single section but also of the overall process compared to the base case simulation model, producing higher quality syngas.
- Gas-pressurized torrefaction decreases the overall performance of the process since it promotes lower energy and carbon yields due to a higher decomposition of the biomass. On the other hand, better performances in terms of natural gas consumption and energy concentration can be achieved. For these reasons, GP torrefaction is better suited for a de-centralized pre-treatment conversion process.

The work contributes to the building of a process model focused on gas-pressurized torrefaction and plasma gasification, leading to further research on these processes. In particular, the study lays the basis for future investigations:

- The effect of the product of a de-centralized GP torrefaction process could be assessed on the treatment and post-treatment process. If in a GP torrefaction the natural gas employed is lower it could bring a positive impact on the overall cost of the plant and also in the CO_2 emissions
- The effect of the utilization of a different plasma gas for the generation of plasma in the gasification process can be studied and compare among each other and with other allothermal gasification technologies.
- Different feedstock with different compositions could be used to assess the most suitable one and their impact on KPI

Bibliography

[1] N. Agon. "Development and study of different numerical plasma jet models and experimental study of plasma gasification of waste." PhD thesis. Jan. 2015.

[2] A. A. Ahmad, N. A. Zawawi, F. H. Kasim, A. Inayat, and A. Khasri. "Assessing the gasification performance of biomass: A review on biomass gasification process conditions, optimization and economic evaluation." In: *Renewable and Sustainable Energy Reviews* 53 (2016), pp. 1333–1347.

[3] "An overview of Fischer-Tropsch Synthesis: XtL processes, catalysts and reactors." In: *Applied Catalysis A: General* 608 (2020), p. 117740.

[4] M. Aneke and M. Wang. "Thermodynamic Comparison of alternative Biomass Gasification Techniques for producing Syngas for Gas Turbine Application." In: *Energy Procedia* 142 (Dec. 2017), pp. 829–834. DOI: 10.1016/j.egypro.2017.12.133.

[5] U. Arena. "Process and technological aspects of municipal solid waste gasification. A review." In: *Waste Management* 32.4 (2012). Solid Waste Gasification, pp. 625–639. ISSN: 0956-053X. DOI: https://doi.org/10.1016/j.wasman.2011.09.025.

[6] Aspen. *Aspen Physical Property System-Physical Property Methods*. Aspen Technology, Inc., 2013.

[7] Aspen. *Aspen Plus-Getting Started Modeling Processes with Solids*. Aspen Technology, Inc., 2013.

[8] S. G. Azevedo, T. Sequeira, M. Santos, and L. Mendes. "Biomass-related sustainability: A review of the literature and interpretive structural modeling." In: *Energy* 171 (2019), pp. 1107–1125. ISSN: 0360-5442. DOI: https://doi.org/10.1016/j.energy.2019.01.068.

[9] Q.-V. Bach, Ø. Skreiberg, and C.-J. Lee. "Process modeling and optimization for torrefaction of forest residues." In: *Energy* 138 (Dec. 2017). DOI: 10.1016/j.energy.2017.07.040.

[10] Q.-V. Bach, Ø. Skreiberg, and C.-J. Lee. "Process modeling for torrefaction of birch branches." In: *Energy Procedia* 142 (Dec. 2017), pp. 395–400. DOI: 10.1016/j.egypro.2017.12.062.

[11] D. Bacovsky, C. Dißauer, B. Drosg, M. Kuba, D. Matschegg, C. Schmidl, E. Carlon, F. Schipfer, F. Kraxner, and V. Djemelinskaia. "How bioenergy contributes to a sustainable future." In: *BIOENERGY REVIEW 2023* (2022).

[12] R. Bates and A. Ghoniem. "Modeling kinetics-transport interactions during biomass torrefaction: The effects of temperature, particle size, and moisture content." In: *Fuel* 137 (Dec. 2014), pp. 216–229. DOI: 10.1016/j.fuel.2014.07.047.

[13] D. A. Bell, B. F. Towler, and M. Fan. *Coal gasification and its applications*. William Andrew, 2010.

[14] P. Bergman, A. Boersma, J. Kiel, M. Prins, K. Ptasinski, and F. Janssen. "Torrefaction for Entrained Flow Gasification of Biomass." In: *Journal of Applied Mechanics-transactions of The Asme - J APPL MECH* (Jan. 2005).

[15] P. Bergman, A. Boersma, R. Zwart, and J. Kiel. "Torrefaction for Biomass Co-Firing in Existing Coal-Fired Power Stations." In: *Energy research Centre of the Netherlands* (Jan. 2005).

[16] P. Bergman, A. Boersma, R. Zwart, and J. Kiel. "Torrefaction for Biomass Co-Firing in Existing Coal-Fired Power Stations." In: *Energy research Centre of the Netherlands* (Jan. 2005).

[17] A. W. Bhutto, A. A. Bazmi, and G. Zahedi. "Underground coal gasification: From fundamentals to applications." In: *Progress in Energy and Combustion Science* 39.1 (2013), pp. 189–214.

[18] M. Cremers, J. Koppejan, J. Middelkamp, J. Witkamp, S. Sokhansanj, S. Melin, and S. Madrali. "Status overview of torrefaction technologies, A review of the commercialisation status of biomass torrefaction." In: (2015).

[19] O. Dacres, S. Tong, X. Li, Y. Sun, F. Wang, G. Luo, H. Liu, H. Hu, and H. Yao. "Gas-pressurized torrefaction of biomass wastes: The effect of varied pressure on pyrolysis kinetics and mechanism of torrefied biomass." In: *Fuel* 276 (Sept. 2020), p. 118132. DOI: 10.1016/j.fuel.2020.118132.

[20] O. Dacres, S. Tong, X. Li, X. Zhu, E. Edreis, H. Liu, G. Luo, N. Worasuwannarak, S. Kerdsuwan, B. Fungtammasan, and H. Yao. "Pyrolysis kinetics of biomasses pretreated by gas-pressurized torrefaction." In: *Energy Conversion and Management* 182 (Feb. 2019), pp. 117–125. DOI: 10.1016/j.enconman.2018.12.055.

[21] M. Dossow. *Simulation and comparison of different synthesis routes for the production of sustainable aviation fuels - a power-and-biomass-to-liquid (PBtL) approach*. 2020.

[22] E. Gucho, K. Shahzad, E. Bramer, N. Akhtar, and G. Brem. "Experimental Study on Dry Torrefaction of Beech Wood and Miscanthus." In: *Energies* 8 (May 2015), pp. 3903–3923. DOI: 10.3390/en8053903.

[23] M. Hansen. *Plasma gasification as an emerging process of thermodynamical recycling: comparison of current concepts*. 2023.

[24] Y. Haseli. "Process Modeling of a Biomass Torrefaction Plant." In: *Energy & Fuels* 32.4 (2018), pp. 5611–5622. DOI: 10.1021/acs.energyfuels.7b03956.

[25] I. Hirka, O. Živný, and M. Hrabovsky. "Numerical Modelling of Wood Gasification in Thermal Plasma Reactor." In: *Plasma Chemistry and Plasma Processing* 37 (July 2017). DOI: 10.1007/s11090-017-9812-z.

[26] Z. Huang, S. Jiang, J. Guo, X. Wang, M. Tan, R. Xiong, Z. Wang, Z. Wu, and H. Li. "Oxidative Torrefaction of Phragmites australis: Gas-Pressurized Effects and Correlation Analysis Based on Color Value." In: *Energy & Fuels* 34.9 (2020), pp. 11073–11082. DOI: 10.1021/acs.energyfuels.0c01974.

[27] B. Ibrahimoglu, A. Cucen, and Z. Yilmazoglu. "Numerical modeling of a downdraft plasma gasification reactor." In: *International Journal of Hydrogen Energy* 42 (July 2016). DOI: 10.1016/j.ijhydene.2016.06.224.

[28] T. Ismail, E. Monteiro, A. Ramos, M. Abd El-Salam, and A. Rouboa. "An Eulerian Model for Forest Residues Gasification in a Plasma Gasifier." In: *Energy International* 182 (June 2019). DOI: 10.1016/j.energy.2019.06.070.

[29] T. Ismail, A. Ramos, M. Abd El-Salam, E. Monteiro, and A. Rouboa. "Plasma fixed bed gasification using an Eulerian model." In: *International Journal of Hydrogen Energy* 44 (Oct. 2019). DOI: 10.1016/j.ijhydene.2019.08.035.

[30] I. Janajreh, S. Raza, and A. Valmundsson. "Plasma gasification process: Modeling, simulation and comparison with conventional air gasification." In: *Energy Conversion and Management* 65 (Jan. 2013), pp. 801–809. DOI: 10.1016/j.enconman.2012.03.010.

[31] Q. Ji, S. Tabassum, S. Hena, C. G. Silva, G. Yu, and Z. Zhang. "A review on the coal gasification wastewater treatment technologies: past, present and future outlook." In: *Journal of Cleaner Production* 126 (2016), pp. 38–55.

[32] M. Kircher. "Sustainability of biofuels and renewable chemicals production from biomass." In: *Current Opinion in Chemical Biology* 29 (2015). Energy • Mechanistic biology, pp. 26–31. ISSN: 1367-5931. DOI: https://doi.org/10.1016/j.cbpa.2015.07.010.

[33] J. Klinger, E. Bar Ziv, and D. Shonnard. "Unified kinetic model for torrefaction–pyrolysis." In: *Fuel Processing Technology* 138 (Oct. 2015). DOI: 10.1016/j.fuproc.2015.05.010.

[34] Y. Kudoh, M. Sagisaka, S. S. Chen, J. C. Elauria, S. H. Gheewala, U. Hasanudin, J. Romero, V. K. Sharma, and X. Shi. "Region-Specific Indicators for Assessing the Sustainability of Biomass Utilisation in East Asia." In: *Sustainability* 7.12 (2015), pp. 16237–16259.

[35] P.-C. Kuo, B. Illathukandy, W. Wu, and J.-S. Chang. "Plasma gasification performances of various raw and torrefied biomass materials using different gasifying agents." In: *Bioresource Technology* 314 (June 2020), p. 123740. DOI: 10.1016/j.biortech.2020.123740.

[36] H.-J. Lee. *Optimization of Fischer-Tropsch plant*. The University of Manchester (United Kingdom), 2011.

[37] M. Li, H. Wang, Z. Huang, X. Yuan, M. Tan, L. Jiang, Z. Wu, X. Qin, and H. Li. "Comparison of atmospheric pressure and gas-pressurized torrefaction of

municipal sewage sludge: Properties of solid products." In: *Energy Conversion and Management* 213 (2020), p. 112793.

[38] K. Liu, Z. Cui, and T. H. Fletcher. "Coal gasification." In: *Hydrogen and syngas production and purification technologies* (2009), pp. 156–218.

[39] Q. Liu, S. C. Chmely, and N. Abdoulmoumine. "Biomass Treatment Strategies for Thermochemical Conversion." In: *Energy & Fuels* 31.4 (2017), pp. 3525–3536. DOI: 10.1021/acs.energyfuels.7b00258.

[40] Q. Liu, S. C. Chmely, and N. Abdoulmoumine. "Biomass Treatment Strategies for Thermochemical Conversion." In: *Energy & Fuels* 31.4 (2017), pp. 3525–3536. DOI: 10.1021/acs.energyfuels.7b00258.

[41] H. Mahmoudi, M. Mahmoudi, O. Doustdar, H. Jahangiri, A. Tsolakis, S. Gu, and M. LechWyszynski. "A review of Fischer Tropsch synthesis process, mechanism, surface chemistry and catalyst formulation." In: *Biofuels Engineering* 2.1 (2017), pp. 11–31. DOI: doi:10.1515/bfuel-2017-0002.

[42] P. Mathieu and R. Dubuisson. "Performance analysis of a biomass gasifier." In: *Energy conversion and management* 43.9-12 (2002), pp. 1291–1299.

[43] L. Mazzoni, M. Almazrouei, C. Ghenai, and I. Janajreh. "A comparison of energy recovery from MSW through plasma gasification and entrained flow gasification." In: *Energy Procedia* 142 (Dec. 2017), pp. 3480–3485. DOI: 10.1016/j.egypro.2017.12.233.

[44] A. J. Minchener. "Coal gasification for advanced power generation." In: *Fuel* 84.17 (2005), pp. 2222–2235.

[45] A. Mishra, S. Gautam, and T. Sharma. "Effect of operating parameters on coal gasification." In: *International Journal of Coal Science & Technology* 5 (2018), pp. 113–125.

[46] P. Mondal, G. Dang, and M. Garg. "Syngas production through gasification and cleanup for downstream applications — Recent developments." In: *Fuel Processing Technology* 92.8 (2011), pp. 1395–1410. ISSN: 0378-3820. DOI: https://doi.org/10.1016/j.fuproc.2011.03.021.

[47] N. Nikolopoulos, R. Isemin, K. Atsonios, D. Kourkoumpas, S. Kuzmin, A. Mikhalev, A. Nikolopoulos, M. Agraniotis, P. Grammelis, and E. Kakaras. "Modeling of wheat straw torrefaction as a preliminary tool for process design." In: *Waste and Biomass Valorization* 4 (2013), pp. 409–420.

[48] Y. Pang, L. Bahr, P. Fendt, L. Zigan, S. Will, T. Hammer, M. Baldauf, R. Fleck, D. Müller, and J. Karl. "Plasma-Assisted Biomass Gasification with Focus on Carbon Conversion and Reaction Kinetics Compared to Thermal Gasification." In: *Energies* 11 (May 2018), p. 1302. DOI: 10.3390/en11051302.

[49] C. Park, U. Zahid, S. Lee, and C. Han. "Effect of process operating conditions in the biomass torrefaction: A simulation study using one-dimensional reactor and process model." In: *Energy* 79 (Jan. 2015). DOI: 10.1016/j.energy.2014.10.085.

[50] E. Peduzzi, G. Boissonnet, G. Haarlemmer, C. Dupont, and F. Maréchal. "Torrefaction modelling for lignocellulosic biomass conversion processes." In: *Energy* 70 (2014), pp. 58–67. ISSN: 0360-5442. DOI: https://doi.org/10.1016/j.energy.2014.03.086.

[51] E. Peduzzi, G. Boissonnet, G. Haarlemmer, C. Dupont, and F. Maréchal. "Torrefaction modelling for lignocellulosic biomass conversion processes." In: *Energy* 70 (2014), pp. 58–67.

[52] J. Popp, Z. Lakner, M. Harangi-Rákos, and M. Fári. "The effect of bioenergy expansion: Food, energy, and environment." In: *Renewable and Sustainable Energy Reviews* 32 (2014), pp. 559–578. ISSN: 1364-0321. DOI: https://doi.org/10.1016/j.rser.2014.01.056.

[53] M. Prins, K. Ptasinski, and F. Janssen. "Torrefaction of wood. Part 2. Analysis of products." In: *Journal of Analytical and Applied Pyrolysis* 77 (Aug. 2006), pp. 35–. DOI: 10.1016/j.jaap.2006.01.001.

[54] M. Rajasekhar, N. Rao, G. Rao, G. Priyadarshini, and N. Kumar. "Energy Generation from Municipal Solid Waste by Innovative Technologies – Plasma Gasification." In: *Procedia Materials Science* 10 (Dec. 2015), pp. 513–518. DOI: 10.1016/j.mspro.2015.06.094.

[55] A. K. Rajvanshi. "Biomass gasification." In: *Alternative energy in agriculture* 2.4 (1986), pp. 82–102.

[56] S. Safarian, R. Unnþórsson, and C. Richter. "A review of biomass gasification modeling." In: *Renewable and Sustainable Energy Reviews* 110 (2019), pp. 378–391.

[57] F. Saleem, A. Rehman, A. Abbas, A. Khoja, F. Ahmad, L. Liu, K. Zhang, and A. Harvey. "A Comparison of the decomposition of biomass gasification tar compound in CO, CO2, H2 and N2 carrier gases using Non-thermal plasma." In: *Journal of the Energy Institute* 97 (Apr. 2021), pp. 161–168. DOI: 10.1016/j.joei.2021.04.013.

[58] S. Sansaniwal, M. Rosen, and S. Tyagi. "Global challenges in the sustainable development of biomass gasification: An overview." In: *Renewable and Sustainable Energy Reviews* 80 (2017), pp. 23–43.

[59] L. Shang, J. Ahrenfeldt, J. Holm, L. Bach, W. Stelte, and U. Henriksen. "Kinetic model for torrefaction of wood chips in a pilot-scale continuous reactor." In: *Journal of Analytical and Applied Pyrolysis* 108 (July 2014). DOI: 10.1016/j.jaap.2014.05.010.

[60] L. Shi, Z. Hu, X. Li, S. Li, L. Yi, X. Wang, H. Hu, G. Luo, and H. Yao. "Gas-pressurized torrefaction of lignocellulosic solid wastes: Low-temperature deoxygenation and chemical structure evolution mechanisms." In: *Bioresource technology* 385 (June 2023), p. 129414. DOI: 10.1016/j.biortech.2023.129414.

[61] M. Stelt, H. Gerhauser, J. Kiel, and K. Ptasinski. "Biomass Upgrading by Torrefaction for the Production of Biofuels: A Review." In: 35 (July 2011), pp. 3748–3762. DOI: 10.1016/j.biombioe.2011.06.023.

[62] Y. Sun, S. Tong, X. Li, F. Wang, Z. Hu, O. D. Dacres, E. M. Edreis, N. Worasuwannarak, M. Sun, H. Liu, H. Hu, G. Luo, and H. Yao. "Gas-pressurized torrefaction of biomass wastes: The optimization of pressurization condition and the pyrolysis of torrefied biomass." In: *Bioresource Technology* 319 (2021), p. 124216. ISSN: 0960-8524. DOI: https://doi.org/10.1016/j.biortech.2020.124216.

[63] D. Sutton, B. Kelleher, and J. R. Ross. "Review of literature on catalysts for biomass gasification." In: *Fuel processing technology* 73.3 (2001), pp. 155–173.

[64] M. Tan, L. Hui, Z. Huang, Z. Wang, R. Xiong, S. Jiang, Z. Wu, C.-Z. Li, and L. Luo. "Comparison of atmospheric and gas-pressurized oxidative torrefaction of heavy-metal-polluted rice straw." In: *Journal of Cleaner Production* 283 (Oct. 2020), p. 124636. DOI: 10.1016/j.jclepro.2020.124636.

[65] S. Tong, L. Xiao, X. Li, X. Zhu, H. Liu, G. Luo, N. Worasuwannarak, S. Kerdsuwan, B. Fungtammasan, and H. Yao. "A gas-pressurized torrefaction method for biomass wastes." In: *Energy Conversion and Management* 173 (2018), pp. 29–36. ISSN: 0196-8904. DOI: https://doi.org/10.1016/j.enconman.2018.07.051.

[66] S. Tong, L. Xiao, X. Li, X. Zhu, H. Liu, G. Luo, N. Worasuwannarak, S. Kerdsuwan, B. Fungtammasan, and H. Yao. "A gas-pressurized torrefaction method for biomass wastes." In: *Energy Conversion and Management* 173 (Oct. 2018), pp. 29–36. DOI: 10.1016/j.enconman.2018.07.051.

[67] J. S. Tumuluru, S. Sokhansanj, J. Hess, C. Wright, and R. Boardman. "A Review on Biomass Torrefaction Process and Product Properties for Energy Applications." In: *Industrial Biotechnology* 7 (Oct. 2011), pp. 384–401. DOI: 10.1089/ind.2011.7.384.

[68] M. van der Stelt, H. Gerhauser, J. Kiel, and K. Ptasinski. "Biomass upgrading by torrefaction for the production of biofuels: A review." In: *Biomass and Bioenergy* 35.9 (2011), pp. 3748–3762. ISSN: 0961-9534. DOI: https://doi.org/10.1016/j.biombioe.2011.06.023.

[69] S. V. Vassilev, D. Baxter, L. K. Andersen, and C. G. Vassileva. "An overview of the chemical composition of biomass." In: *Fuel* 89.5 (2010), pp. 913–933. ISSN: 0016-2361. DOI: https://doi.org/10.1016/j.fuel.2009.10.022.

[70] N. J. Wagner, M. Coertzen, R. H. Matjie, and J. C. van Dyk. "Coal gasification." In: *Applied coal petrology*. Elsevier, 2008, pp. 119–144.

[71] P. J. Woolcock and R. C. Brown. "A review of cleaning technologies for biomass-derived syngas." In: *Biomass and Bioenergy* 52 (2013), pp. 54–84. ISSN: 0961-9534. DOI: https://doi.org/10.1016/j.biombioe.2013.02.036.

[72] L. Xiao, X. Zhu, X. Li, Z. Zhang, R. Ashida, K. Miura, G. Luo, W. Liu, and H. Yao. "Effect of Pressurized Torrefaction Pretreatments on Biomass CO2 Gasification." In: *Energy & Fuels* 29 (Oct. 2015). DOI: 10.1021/acs.energyfuels.5b01485.

A. Appendix

Table A.1.: Simulation components

Component ID	Type	Component name	Alias
MIS	Nonconventional		
BEECH	Nonconventional		
TORMIS	Nonconventional		
TORBECH	Nonconventional		
H2O	Conventional	WATER	H2O
CO2	Conventional	CARBON-DIOXIDE	CO2
N2	Conventional	NITROGEN	N2
O2	Conventional	OXYGEN	O2
CO	Conventional	CARBON-MONOXIDE	CO
CH3OH	Conventional	METHANOL	CH4O
CH3COOH	Conventional	ACETIC-ACID	C2H4O2-1
CH2O2	Conventional	FORMIC-ACID	CH2O2
LACTI-01	Conventional	LACTIC-ACID	C3H6O3-D1
CH4	Conventional	METHANE	CH4
NH3	Conventional	AMMONIA	H3N
H2	Conventional	HYDROGEN	H2
ASH	Nonconventional		
C	Solid	CARBON-GRAPHITE	C
CL2	Conventional	CHLORINE	CL2
S	Conventional	SULFUR	S

continued on next page

continued from previous page

HCN	Conventional	HYDROGEN-CYANIDE	CHN
H2S	Conventional	HYDROGEN-SULFIDE	H2S
COS	Conventional	CARBONYL-SULFIDE	COS
NO	Conventional	NITRIC-OXIDE	NO
HCL	Conventional	HYDROGEN-CHLORIDE	HCL
CL	Conventional	CHLORINE-MONATOMIC-GAS	CL
HCLO	Conventional	HYPOCHLOROUS-ACID	HCLO
SO2	Conventional	SULFUR-DIOXIDE	O2S
NH4+	Conventional	NH4+	NH4+
OH-	Conventional	OH-	OH-
CLO-	Conventional	CLO-	CLO-
H3O+	Conventional	H3O+	H3O+
CL-	Conventional	CL-	CL-
CN-	Conventional	CN-	CN-
SO3–	Conventional	SO3–	SO3-2
HSO3-	Conventional	HSO3-	HSO3-
HCO3-	Conventional	HCO3-	HCO3-
NH2COO-	Conventional	CARBAMATE	NH2COO-
S–	Conventional	S–	S-2
CO3–	Conventional	CO3–	CO3-2
HS-	Conventional	HS-	HS-
DEPG5	Conventional	PENTAETHYLENE-GLYCOL-DIMETHYL-ET	C12H26O6
CS2	Conventional	CARBON-DISULFIDE	CS2
S2	Conventional	SULFUR-DIATOMIC	S2
AR	Conventional	ARGON	AR
C2H4	Conventional	ETHYLENE	C2H4
C3H6	Conventional	PROPYLENE	C3H6-2
C4H8	Conventional	1-BUTENE	C4H8-1
C5H10	Conventional	1-PENTENE	C5H10-2

continued on next page

continued from previous page

C6H12	Conventional	1-HEXENE	C6H12-3
C7H14	Conventional	1-HEPTENE	C7H14-7
C8H16	Conventional	1-OCTENE	C8H16-16
C9H18	Conventional	1-NONENE	C9H18-3
C10H20	Conventional	1-DECENE	C10H20-5
C11H22	Conventional	1-UNDECENE	C11H22-2
C12H24	Conventional	1-DODECENE	C12H24-2
C13H26	Conventional	1-TRIDECENE	C13H26-2
C14H28	Conventional	1-TETRADECENE	C14H28-2
C15H30	Conventional	1-PENTADECENE	C15H30-2
C16H32	Conventional	1-HEXADECENE	C16H32-2
C17H34	Conventional	1-HEPTADECENE	C17H34-D1
C18H36	Conventional	1-OCTADECENE	C18H36-1
C19H38	Conventional	1-NONADECENE	C19H38-D1
C20H40	Conventional	1-EICOSENE	C20H40-D1
C21H42	Conventional	1-HENEICOSENE	C21H42-N2
C22H44	Conventional	1-DOCOSENE	C22H44-D1
C23H46	Conventional	1-TRICOSENE	C23H46-N3
C24H48	Conventional	1-TETRACOSENE	C24H48-D1
C25H50	Conventional	C25H50	C25H50
C26H52	Conventional	1-HEXACOSENE	C26H52-N10
C27H54	Conventional	1-HEPTACOSENE	C27H54-N3
C28H56	Conventional	1-OCTACOSENE	C28H56-N2
C29H58	Conventional	1-NONACOSENE	C29H58
C30H60	Conventional	1-TRIACONTENE	C30H60
C40H80	Conventional	1-TETRACONTENE	C40H80
METHA-01	Conventional	METHANE	CH4
C2H6	Conventional	ETHANE	C2H6
C3H8	Conventional	PROPANE	C3H8

continued on next page

continued from previous page

C4H10	Conventional	N-BUTANE	C4H10-1
C5H12	Conventional	N-PENTANE	C5H12-1
C6H14	Conventional	N-HEXANE	C6H14-1
C7H16	Conventional	N-HEPTANE	C7H16-1
C8H18	Conventional	N-OCTANE	C8H18-1
C9H20	Conventional	N-NONANE	C9H20-1
C10H22	Conventional	N-DECANE	C10H22-1
C11H24	Conventional	N-UNDECANE	C11H24
C12H26	Conventional	N-DODECANE	C12H26
C13H28	Conventional	N-TRIDECANE	C13H28
C14H30	Conventional	N-TETRADECANE	C14H30
C15H32	Conventional	N-PENTADECANE	C15H32
C16H34	Conventional	N-HEXADECANE	C16H34
C17H36	Conventional	N-HEPTADECANE	C17H36
C18H38	Conventional	N-OCTADECANE	C18H38
C19H40	Conventional	N-NONADECANE	C19H40
C20H42	Conventional	N-EICOSANE	C20H42
C21H44	Conventional	N-HENEICOSANE	C21H44
C22H46	Conventional	N-DOCOSANE	C22H46
C23H48	Conventional	N-TRICOSANE	C23H48
C24H50	Conventional	N-TETRACOSANE	C24H50
C25H52	Conventional	N-PENTACOSANE	C25H52
C26H54	Conventional	N-HEXACOSANE	C26H54
C27H56	Conventional	N-HEPTACOSANE	C27H56
C28H58	Conventional	N-OCTACOSANE	C28H58
C29H60	Conventional	N-NONACOSANE	C29H60
C30H62	Conventional	N-TRIACONTANE	C30H62
C72H146	Conventional	DOHEPTACONTANE	C72H146

Table A.2.: Pretreatment simulation blocks

Block	Specification
R-DRYER (RStoic)	Pressure: 1 bar Outlet temperature determined by design specification
COOL-P (Heater)	Pressure: isobaric Outlet temperature:
DRY-SEP (Cyclon)	Pressure: 1 bar Temperature change: 0°C Model: solid separator Fraction of solid to solid output: 1 Fraction of Vapor to vapor outlet:1
SPLITTER (FSplit)	Split fraction REC1: 0.3 Split fraction REC2: from design specification
MIXER (Mixer)	No specification
R-TORR (RStoic)	Flash type: Temp. Temperature: 20°C
TOR-SEP (Cyclon)	Pressure: 1 bar Temperature change: 0°C Model: solid separetor Fraction of solid to solid output: 1 Fraction of Vapor to vapor outlet:1
R-COMB (RStoic)	Isobaric Combustion reactions with NOx generation

Continued on next page

Continuation from previous Table

Block	Specification
HEX (HeatX)	Model Fidelity: Shortcut Shortcut flow direction: cuntercurrent Calculation Mode: design, Specification: Hot stream outlet temperature Temperature: 35°C, Min. temp. approach: 1°C
GRINDER (Crusher)	Select Equipment Crusher type: Multiple roll SelectionBreakage functions: US Bureau of Mines

Table A.3.: Gasification simulation blocks

Block	Specification
R-PYRO (RYield)	Adiabatic and isobaric
R-NIT (RStoic)	Adiabatic and isobaric
R-GAS (RGibbs)	Calculation options: Restrict chemical equilibrium - specify temperature approach or reaction extents Pressure: 37 bar Temperature approach for the entire system: -400 K
C1 (Compr)	Isentropic Compressor Discharge Pressure: 8 bar
C2 (Compr)	Isentropic Compressor Discharge Pressure: 37 bar
C3 (Compr)	As block C1
C4 (Compr)	As block C2
COOLER-1 (Heater)	Temperature: 50 °C Isobaric
COOLER-2 (Heater)	As block COOLER-1

Continued on next page

Continuation from previous Table

Block	Specification
COOL3 (Heater)	As block COOLER-1

Table A.4.: Quench simulation blocks

Block	Specification
P1 (Pump)	Discharge pressure: 36 bar
SPLITTER (FSplit)	Split fraction SP-2-SC: 0.1
R-QUENCH (Flash2)	Pressure: -1 bar Adiabatic
SLAG-SEP (HyCyc)	Model: Solid separator Fraction of solid to solid outlet: 1 Liquid load of solid outlet: 0.3
SCRUBBER (Sep)	Split fractions for outlet stream **SCR-OUT** specified as in table A.10
Sep (Flash2)	Isobaric Adiabatic
P2 (Pump)	Pressure increase : 1 bar

Table A.5.: AGR simulation blocks

Block	Specification
COMP1 (Compr)	Isentropic Compressor Discharge Pressure: 54 bar
COOL1 (Heater)	Temperature: 38°C Isobaric

Continued on next page

Continuation from previous Table

Block	Specification
ABS-H2S (Sep2)	Inlet Flash Pressure: 53.5 bar Outlet flash Pressure: 53.5 bar Outlet flash Temperature: 22.7 °C (S-OUT2), 17°C (GAS) Split fraction in table A.12
C3 (Heater)	Temperature: 10°C Isobaric
C1 (Heater)	Temperature: 30°C Isobaric
P2 (Pump)	Pressure increase: 2 bar
C2 (Heater)	Temperature: 105°C Isobaric
CN (Pump)	Isentropic Compressor Discharge Pressure: 54 bar
COOLN (Heater)	Temperature: 93°C Isobaric
CONC-H2S (Sep2)	Inlet Flash Pressure: 54 bar Outlet flash Pressure: 54 bar Outlet flash Temperature: 99 °C (SRICH2), 103.4°C (REC) Split fraction in table A.13
B11 (Sep2)	Outlet flash Pressure: 2.1 bar Outlet flash Temperature: 49 °C (WASTE), 10°C (SOL-LEAN)
COOL-1 (Heater)	Isobaric
COOL-L (Heater)	Temperature: 10°C Isobaric
MIX (Mixer)	Isobaric

Continued on next page

Continuation from previous Table

Block	Specification
CO2-ABS (RadFrac)	See Table A.14
PURIFY (Sep2)	H_2S molar fraction: 9e-9
SPLIT (FSplit)	Isobaric
P1 (Pump)	Discharge Pressure: 54 bar
COOL-S (Heater)	Temperature: 10°C Isobaric
PS (Pump)	Discharge Pressure: 52.7 bar
HPF (Flash2)	Adiabatic Pressure:....
MPF (Flash2)	Adiabatic Pressure: determined by design specification
LPF (Flash2)	Adiabatic Pressure: 1.5 bar
C-H (Compr)	Adiabatic Discharge pressure: 54 bar
COOL-H (Heater)	Temperature: 30°C Pressure: -1
KNOCKOUT (Flash2)	Temperature: 30°C Isobaric

Table A.8.: R-FT reactions

N.	Reactions	CO Conversion
Parafins reactions		
1	$CO + 3\ H_2 \longrightarrow CH_4 + H_2O$	0.015129
2	$2\ CO + 5\ H_2 \longrightarrow C_2H_6 + 2\ H_2O$	0.015129
3	$3\ CO + 7\ H_2 \longrightarrow C_3H_8 + 3\ H_2O$	0.015129

Continuation of Table

N.	Reactions	CO Conversion
4	$4\ CO + 9\ H_2 \longrightarrow C_4H_{10} + 4\ H_2O$	0.015129
5	$5\ CO + 11\ H_2 \longrightarrow C_5H_{12} + 5\ H_2O$	0.015129
6	$6\ CO + 13\ H_2 \longrightarrow C_6H_{14} + 6\ H_2O$	0.015129
7	$7\ CO + 15\ H_2 \longrightarrow C_7H_{16} + 7\ H_2O$	0.015129
8	$8\ CO + 17\ H_2 \longrightarrow C_8H_{18} + 8\ H_2O$	0.015129
9	$9\ CO + 19\ H_2 \longrightarrow C_9H_{20} + 9\ H_2O$	0.015129
10	$10\ CO + 21\ H_2 \longrightarrow C_{10}H_{22} + 10\ H_2O$	0.015129
11	$11\ CO + 23\ H_2 \longrightarrow C_{11}H_{24} + 11\ H_2O$	0.015129
12	$12\ CO + 25\ H_2 \longrightarrow C_{12}H_{26} + 12\ H_2O$	0.015129
13	$13\ CO + 27\ H_2 \longrightarrow C_{13}H_{28} + 13\ H_2O$	0.015129
14	$14\ CO + 29\ H_2 \longrightarrow C_{14}H_{30} + 14\ H_2O$	0.015129
15	$15\ CO + 31\ H_2 \longrightarrow C_{15}H_{32} + 15\ H_2O$	0.015129
16	$16\ CO + 33\ H_2 \longrightarrow C_{16}H_{34} + 16\ H_2O$	0.015129
17	$17\ CO + 35\ H_2 \longrightarrow C_{17}H_{36} + 17\ H_2O$	0.015129
18	$18\ CO + 37\ H_2 \longrightarrow C_{18}H_{38} + 18\ H_2O$	0.015129
19	$19\ CO + 39\ H_2 \longrightarrow C_{19}H_{40} + 19\ H_2O$	0.015129
20	$20\ CO + 41\ H_2 \longrightarrow C_{20}H_{42} + 20\ H_2O$	0.015129
21	$21\ CO + 43\ H_2 \longrightarrow C_{21}H_{44} + 21\ H_2O$	0.015129
22	$22\ CO + 45\ H_2 \longrightarrow C_{22}H_{46} + 22\ H_2O$	0.015129
23	$23\ CO + 47\ H_2 \longrightarrow C_{23}H_{48} + 23\ H_2O$	0.015129
24	$24\ CO + 49\ H_2 \longrightarrow C_{24}H_{50} + 24\ H_2O$	0.015129
25	$25\ CO + 51\ H_2 \longrightarrow C_{25}H_{52} + 25\ H_2O$	0.015129
26	$26\ CO + 53\ H_2 \longrightarrow C_{26}H_{54} + 26\ H_2O$	0.015129
27	$27\ CO + 55\ H_2 \longrightarrow C_{27}H_{56} + 27\ H_2O$	0.015129
28	$28\ CO + 57\ H_2 \longrightarrow C_{28}H_{58} + 28\ H_2O$	0.015129
29	$29\ CO + 59\ H_2 \longrightarrow C_{29}H_{60} + 29\ H_2O$	0.015129
30	$30\ CO + 61\ H_2 \longrightarrow C_{30}H_{62} + 30\ H_2O$	0.015129
31	$72\ CO + 145\ H_2 \longrightarrow C_{72}H_{146} + 72\ H_2O$	0.015129
Olefins reactions		
32	$2\ CO + 4\ H_2 \longrightarrow C_2H_4 + 2\ H_2O$	0.001250664

Continuation of Table

N.	Reactions	CO Conversion
33	$3\ CO + 6\ H_2 \longrightarrow C_3H_6 + 3\ H_2O$	0.001250664
34	$4\ CO + 8\ H_2 \longrightarrow C_4H_8 + 4\ H_2O$	0.001250664
35	$5\ CO + 10\ H_2 \longrightarrow C_5H_{10} + 5\ H_2O$	0.001250664
36	$6\ CO + 12\ H_2 \longrightarrow C_6H_{12} + 6\ H_2O$	0.001250664
37	$7\ CO + 14\ H_2 \longrightarrow C_7H_{14} + 7\ H_2O$	0.001250664
38	$8\ CO + 16\ H_2 \longrightarrow C_8H_{16} + 8\ H_2O$	0.001250664
39	$9\ CO + 18\ H_2 \longrightarrow C_9H_{18} + 9\ H_2O$	0.001250664
40	$10\ CO + 20\ H_2 \longrightarrow C_{10}H_{20} + 10\ H_2O$	0.001250664
41	$11\ CO + 22\ H_2 \longrightarrow C_{11}H_{22} + 11\ H_2O$	0.001250664
42	$12\ CO + 24\ H_2 \longrightarrow C_{12}H_{24} + 12\ H_2O$	0.001250664
43	$13\ CO + 26\ H_2 \longrightarrow C_{13}H_{26} + 13\ H_2O$	0.001250664
44	$14\ CO + 28\ H_2 \longrightarrow C_{14}H_{28} + 14\ H_2O$	0.001250664
45	$15\ CO + 30\ H_2 \longrightarrow C_{15}H_{30} + 15\ H_2O$	0.001250664
46	$16\ CO + 32\ H_2 \longrightarrow C_{16}H_{32} + 16\ H_2O$	0.001250664
47	$17\ CO + 34\ H_2 \longrightarrow C_{17}H_{34} + 17\ H_2O$	0.001250664
48	$18\ CO + 36\ H_2 \longrightarrow C_{18}H_{36} + 18\ H_2O$	0.001250664
49	$19\ CO + 38\ H_2 \longrightarrow C_{19}H_{38} + 19\ H_2O$	0.001250664
50	$20\ CO + 40\ H_2 \longrightarrow C_{20}H_{40} + 20\ H_2O$	0.001250664
51	$21\ CO + 42\ H_2 \longrightarrow C_{21}H_{42} + 21\ H_2O$	0.001250664
52	$22\ CO + 44\ H_2 \longrightarrow C_{22}H_{44} + 22\ H_2O$	0.001250664
53	$23\ CO + 46\ H_2 \longrightarrow C_{23}H_{46} + 23\ H_2O$	0.001250664
54	$24\ CO + 48\ H_2 \longrightarrow C_{24}H_{48} + 24\ H_2O$	0.001250664
55	$25\ CO + 50\ H_2 \longrightarrow C_{25}H_{50} + 25\ H_2O$	0.001250664
56	$26\ CO + 52\ H_2 \longrightarrow C_{26}H_{52} + 26\ H_2O$	0.001250664
57	$27\ CO + 54\ H_2 \longrightarrow C_{27}H_{54} + 27\ H_2O$	0.001250664
58	$28\ CO + 56\ H_2 \longrightarrow C_{28}H_{56} + 28\ H_2O$	0.001250664
59	$29\ CO + 58\ H_2 \longrightarrow C_{29}H_{58} + 29\ H_2O$	0.001250664
61	$40\ CO + 80\ H_2 \longrightarrow C_{40}H_{80} + 40\ H_2O$	0.001250664
Metanation reaction		
62	$CO + 3\ H_2 \longrightarrow CH_4 + H_2O$	0.04348108

Continuation of Table

N.	Reactions	CO Conversion

End of Table

Table A.6.: FTS simulation blocks

Block	Specification
HEATER (Heater)	Temperature: 220°C Isobaric
R-FT (RStoic)	Isobaric
B2 (Flash2)	Temperature: 25°C Isobaric

Table A.7.: Feedstock torrefied biomass composition in dry basis (db)

Ultimate Analysis				
Component	MIS	BEECH	TORMIS	TORBECH
ASH	1,57	0,65	1,8	0,82
CARBON	45,57	46,008	55,10	53,87
HYDROGEN	5,07	5,174	5,17	5,14
NITROGEN	0,33	0,226	0,41	0,30
SULFUR	0,09	0,065	0,09	0,07
OXYGEN	43,65	44,05	39,22	40,62
Proximal Analysis				
MOISTURE	30	30	3	3
VM	80,38	80,38	55,10	53,87
FC	17,96	18,94	5,17	5,14
ASH	1,66	0,68	1,8	0,82

Table A.9.: Parameters for volatiles fractional conversion equation

Volatiles i	**A**	**B**
CO	1.9454E-22	8.02750079
CO_2	7.0014E-14	4.793320225
CH_3OH	1.6541E-19	6.915418575
CH_3COOH	1.8042E-17	6.270696455
CH_2O_2	5.8785E-16	5.3723280
$C_3H_6O_3$	2.4314E-36	13.739307

Table A.10.: Split fractions of SCR-OUT block

SCR-OUT component	**Split fractions**
HCl	1
CO_2	0
H_2S	0.02
NH_3	0.44
HCN	0.23

Table A.11.: Parameters for volatiles fractional conversion equation

Component j	**Component i**	A_{ij}	B_{ij}	Solubility relative to CO_2 in DEPG5
DEPG5	CO	17.403	-1720.0	1
DEPG5	CO_2	13.828	-1720.0	8.9
DEPG5	H_2S	13.678	-2297.2	$1.31 \cdot 10^{-2}$
DEPG5	H_2	12.402	0	$6.7 \cdot 10^{-2}$
DEPG5	CH_4	16.531	-1720.0	$2.8 \cdot 10^{-2}$
DEPG5	N_2	17.74	-1720.0	$2.0 \cdot 10^{-2}$

Table A.12.: Split fraction for stream GAS in block ABS-H2S

GAS component	**Split fractions**
H_2O	0.006
CO_2	0.85
N_2	0.993
O_2	0.98
CO	0.995
CH_4	0.98
H_2	0.995
NO	0.99

Table A.13.: Split fraction for stream REC in block CONC-H2S

REC component	**Split fractions**
H_2O	0.0001
CO_2	0.99
N_2	0.999
O_2	0.9
CO	1
CH_4	1
H_2	1
H_2S	0.03
$DEPG_5$	0.0001

Table A.14.: CO2-ABS block specifications

Configuration	**Streams**		
Calculation type: equilibrium	Name	Stage	Convention
Number of stages: 12	SOLV-REC	1	Above-Stage
Condenser: none	ABS-IN	12	On-Stage
Reboiler: none	CS-TO-AB	4	Above-Stage

Table A.15.: Feedstock and torrefied biomass composition in dry basis (db) in modification 2 case model

Ultimate Analysis				
Component	MIS	BEECH	TORMIS	TORBECH
ASH	9.6	0.4	18.7	0,8
CARBON	44.2	55.6	55,10	64.9
HYDROGEN	4.7	5.88	4.28	5.46
NITROGEN	0.81	0.04	1.22	0.09
OXYGEN	50.3	44	38.9	29.6
Proximal Analysis				
MOISTURE	30	30	3	3
VM	75.2	85.5	40.8	62.1
FC	15.2	14.1	40.5	37.1
ASH	9.6	0.4	18.7	0.8